Bistability in a Model of Hepatitis B Virus Dynamics

Nazia Afrin[1], Stanca M. Ciupe[2], Jessica M. Conway[3] and Hayriye Gulbudak[1*]

[1]Department of Mathematics, University of Louisiana at Lafayette, 104 E. University Circle Lafayette, Lafayette, 70503, LA, USA.
[2]Department of Mathematics, Virginia Tech, 460 McBryde Hall, Blacksburg, 24060, VA, USA.
[3]Department of Mathematics and department of Biology, PennState, 201 Old Main, University Park, Pennsylvania, 16802, PA, USA.

*Corresponding author(s). E-mail(s): hayriye.gulbudak@louisiana.edu ;

Abstract

Understanding the mechanisms responsible for different clinical outcomes following hepatitis B infection requires a systems investigation of dynamical interactions between the virus and the immune system. To help elucidate mechanisms of protection, we developed a deterministic mathematical model of hepatitis B infection that accounts for cytotoxic immune responses resulting in infected cell death, non-cytotoxic immune responses resulting in infected cell cure and protective immunity from reinfection, and cell proliferation. We analysed the model and presented outcomes based on three important disease markers: the basic reproduction number $\boldsymbol{\mathcal{R}_0}$, the infected cells death rate $\boldsymbol{\delta}$ (describing the effect of cytotoxic immune responses), and the liver carrying capacity $\boldsymbol{K}$ (describing the liver susceptibility to infection). Using asymptotic and bifurcation analysis techniques, we determined regions where virus is cleared, virus persists, and where clearance-persistence is determined by the size of viral inoculum. These results can guide the development of personalized intervention.

Keywords: hepatitis B virus, mathematical modeling, bistability, Hopf bifurcation

1 Introduction

Despite effective vaccines and improved treatment strategies, hepatitis B virus (HBV) continues to be a global health burden with over 3.5% of the world population being chronically infected [1]. HBV spreads vertically from mother to child, through sexual contact and after exposure with infected blood or body fluids [2]. The risk of progression to chronic disease is dependent on host age, viral characteristics, and immune responses. While acute infection is generally cleared in adult immunocompetent patients, up to 90% infants, 50% children younger than five, and 5-10% adults develop chronic infections which lead to liver disease such as cirrhosis and hepatocellular carcinoma [3, 4, 5]. Extensive work has been conducted that focuses on understanding of key immunological interactions, as well as hepatitis B virus molecular dynamics, that dictate the infection outcome [6]. HBV has developed multiple strategies for avoiding innate and adaptive immunity, with hepatitis B e- and s-antigens (HBeAg and HBsAg) being responsible for the suppression of interferon responses [7] and of natural killer cell function [8]; the impairment of dendritic cells [9]; and the exhaustion of cellular T-cell function [10]. Chimpanzee inoculation studies have linked the magnitude of the HBV dose with infection outcomes, which range from no infection, to acute infection (where the entire liver is infected prior to viral clearance), to chronic viral persistence [11]. They determined that the varying outcomes are immune-dependent, with medium inoculum dose leading to CD8 T-cell mediated immune response that synchronize with HBV dynamics and result in low or no liver infection; low inoculum dose leading to improper CD8 T-cell responses, 100% liver infection, and viral persistence; and high inoculum dose resulting in acute infection of the entire liver followed by viral clearance [12, 11]. Understanding the mechanisms responsible for different outcomes requires a systems investigation of dynamical interactions between host and virus (described using theoretical tools, such as mathematical models) in order to provide testable biological hypotheses for the observed empirical outcomes.

Previous modeling work has helped understanding the relationship between inoculum dose, immune responses, cell depletion, and infection outcomes [13] for hepatitis B viral infections [14, 15, 16, 17], HIV [18], respiratory viral infections [19], and vaccine induced immunity [20]. Non-autonomous systems of differential equations, who incorporate time dependent functions for infection rates [17, 21] or immune responses [14] (assumed to be dose dependent), have predicted that delayed immune responses lead to acute infections followed by clearance, weak immune response lead to viral persistence, and strong immune responses block the infection altogether. In autonomous systems of differential equations, however, the dependence of outcomes on initial inoculum, i.e. the

initial condition of the virus concentration variable (rather than parameters or time-dependent functions), requires the presence of bistable dynamics. The target cell limited model of viral infection (see [22, 23, 24, 21] for a review) that assumes interactions between target cells T, infected cells I and virus V according to the following system:

$$\begin{aligned} \frac{dT}{dt} &= s - \beta TV - dT, \\ \frac{dI}{dt} &= \beta TV - \delta I, \\ \frac{dV}{dt} &= pI - cV, \end{aligned} \tag{1}$$

predicts no infection when $R_0 = \frac{sp\beta}{d\delta c} < 1$ and viral persistence when $R_0 > 1$, regardless of initial conditions. In this paper, we show that an extended autonomous system, incorporating additional hepatitis B-specific viral-host mechanisms into the model Eq. (1), such as the proliferation of uninfected and infected cells [25, 26, 16, 27], cytolytic and non-cytolytic immune responses [25, 26, 15], and the emergence of cured cells that are protected to reinfection [26, 28], results in bistable dynamics. Here, we determine conditions for bistability and investigate the relationship between inoculum dose and model outcomes. Armed with these insights, we propose target mechanisms and interventions that induce viral clearance.

2 Immunological model of HBV

We expand the classical viral dynamics model Eq. (1) by assuming the interaction between hepatitis B virus (V) and three classes of liver cells (hepatocytes - the main target of hepatitis B virus): uninfected (T), infected (I), and protected from (refractory to) reinfection cells (P). We model homeostatic proliferation of each hepatocyte family via logistic growth rates with the same carrying capacity K and different per capita proliferation rates r_T, r_I, and r_P for uninfected, infected, and protected cells, respectively. In addition, we assume that uninfected hepatocytes die naturally at per capita rate d. Upon interaction with virus, target cells become infected at rate β and infected cells are removed via either immune-mediated killing at rate δ or immune-mediated cure that moves them into the protected class at rate ρ. In addition, infected cells produce π virions per day and virus is cleared at rate c. Lastly, the immune-protected state of class P wanes at rate μ. A model diagram for these interactions is given in Figure (1) and the corresponding autonomous system

of differential equations, describing these interactions is given by:

$$\begin{aligned}
\text{Target} \quad \frac{dT}{dt} &= \overbrace{r_T T\left(1-\frac{T+I+P}{K}\right)}^{\text{logistic growth}} - \overbrace{\beta TV}^{\text{absorption}} + \overbrace{\mu P}^{\text{waning}} - \overbrace{dT}^{\text{death}} \\
\text{Infected} \quad \frac{dI}{dt} &= \overbrace{r_I I\left(1-\frac{T+I+P}{K}\right)}^{\text{logistic growth}} + \overbrace{\beta TV}^{\text{absorption}} - \overbrace{\rho I}^{\text{cure}} - \overbrace{\delta I}^{\text{death}} \\
\text{Protected} \quad \frac{dP}{dt} &= \overbrace{r_P P\left(1-\frac{T+I+P}{K}\right)}^{\text{logistic growth}} + \overbrace{\rho I}^{\text{cure}} - \overbrace{\mu P}^{\text{waning}} \\
\text{Free virus} \quad \frac{dV}{dt} &= \overbrace{\pi I}^{\text{virus prod.}} - \overbrace{cV}^{\text{clearance}} - \overbrace{\beta TV}^{\text{absorption}} .
\end{aligned} \tag{2}$$

The initial conditions are $T(0) = T_0$, $I(0) = 0$, $V(0) = V_0$ and $P(0) = 0$.

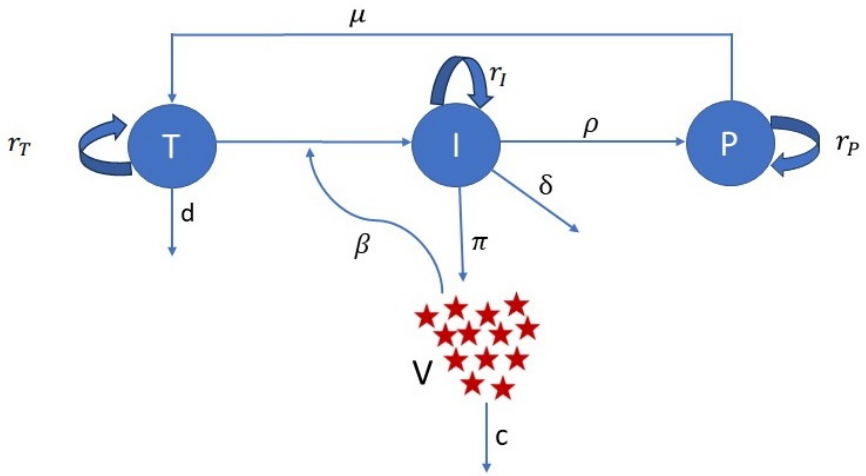

Fig. 1 Diagram for model Eq. (2), where T, I, P, and V represent the uninfected cells, infected cells, protected from reinfection cells, and free viruses, respectively.

Next, we will investigate the long-term dynamics of model Eq. (2) via stability analysis. Moreover, we will determine relationships between outcomes of model dynamics, parameters, and initial conditions via both bifurcation and threshold analysis along with numerical simulations similar to previous studies [29, 30, 31, 32, 33].

3 Threshold dynamics, equilibria, and bifurcation analysis

The analytical results suggest that the model Eq. (2) has three boundary equilibria. The first boundary equilibrium is the trivial equilibrium

$$\mathcal{E}_0^0 = (0, 0, 0, 0),$$

corresponding to clearance of infection in the presence of liver failure. It exists for all model parameters. The second boundary equilibrium is the infection-free equilibrium (IFE)

$$\mathcal{E}_0 = (\overline{T}^0, 0, 0, 0),$$

where $\overline{T}^0 = K(1 - \frac{d}{r_T})$. It is biologically relevant if and only if the uninfected cells' per capita division rate exceeds their per capita death rate, i.e. $r_T > d$.

Remark 1 Here we introduce existence conditions guaranteeing the positivity of equilibria:

(a) Let

$$\overline{T}^0 = K\left(1 - \frac{d}{r_T}\right)$$

be the concentrations of uninfected liver cells in the absence of virus. It is positive if and only if $\frac{r_T}{d} > 1$,

(b) Let

$$\overline{I}^0 = K\left(1 - \frac{\delta + \rho}{r_I}\right)$$

be the concentrations of infected liver cells in the absence of virus. It is positive if and only if $\frac{r_I}{\delta+\rho} > 1$,

(c) Let

$$\overline{P}^0 = K\left(1 - \frac{\mu}{r_P}\right)$$

be the concentrations of protected liver cells in the absence of virus. It is positive if and only if $\frac{r_P}{\mu} > 1$,

(d) The concentration of protected liver cells exceeds the concentration of uninfected liver cells in the absence of the virus,

$$\overline{P}^0 > \overline{T}^0,$$

if and only if $\frac{r_P}{\mu} > \frac{r_T}{d}$.

The viral clearance is the desired outcome of any exposure to hepatitis B virus. The third boundary equilibrium is the clearance with immunity equilibrium (ClImE)

$$\mathcal{E}_0^{cl} = (\overline{T}^*, 0, \overline{P}^*, 0),$$

where $\overline{T}^* = \frac{\overline{P}^0}{1+\frac{r_T}{K\mu}(\overline{P}^0-\overline{T}^0)}$, and $\overline{P}^* = \frac{r_T}{K\mu}(\overline{P}^0-\overline{T}^0)\overline{T}^*$. It is biologically relevant if and only if the per capita division rate of the protected cells over their lifespan is bigger than the per capita division rate of the uninfected cells over their lifespan and the per capita division rate of the protected cells is bigger than their per capita death rate i.e. $\frac{r_P}{\mu} > \min\left\{1, \frac{r_T}{d}\right\}$ (alternatively, $\overline{P}^0 > \min\{0, \overline{T}^0\}$, see Remark 1).

Lastly, model Eq. (2) has up to three biologically feasible interior equilibria, corresponding to different types of chronic infection equilibrium (CIE)

$$\mathcal{E}_i^{\dagger} = (\overline{T}_i^{\dagger}, \overline{I}_i^{\dagger}, \overline{P}_i^{\dagger}, \overline{V}_i^{\dagger}), i = 1, 2, 3.$$

Their general expressions and conditions for existence will be presented in theorem 4 and proposition 5.

Table 1 Equilibria and conditions for their local stability

Equilibrium			Notation	$(\overline{T}, \overline{I}, \overline{P}, \overline{V})$ and the existence condition(s)*	Threshold condition(s)
Boundary	(i)	Clearance with liver failure equilibrium	$\mathcal{E}_0^0$	$(0, 0, 0, 0)$	$\max\left\{\frac{r_T}{d}, \frac{r_I}{\delta+\rho}, \frac{r_P}{\mu}\right\} < 1$ (see proposition 1)
Boundary	(ii)	Infection-free equilibrium (IFE)	$\mathcal{E}_0$	$(\overline{T}^0, 0, 0, 0)$, where $\overline{T}^0 = K(1 - \frac{d}{r_T})$	$\mathcal{R}_0 < 1$, where $\mathcal{R}_0 = \frac{r_I}{(\delta+\rho)}(1 - \frac{\overline{T}^0}{K}) + \frac{\pi}{(\delta+\rho)} \frac{\beta\overline{T}^0}{(c+\beta\overline{T}^0)}$ (see theorem 2)
Coexistence	(iii)	Clearance with immunity equilibrium (ClImE)	$\mathcal{E}_0^{cl}$	$(\overline{T}^*, 0, \overline{P}^*, 0)$, where $\overline{T}^* = \frac{\overline{P}^0}{1+\frac{r_T}{K\mu}(\overline{P}^0 - \overline{T}^0)}$, $\overline{P}^* = \frac{r_T}{K\mu}(\overline{P}^0 - \overline{T}^0)\overline{T}^*$	$\frac{r_P}{\mu} > \frac{r_I}{\delta+\rho-\pi}$ (see theorem 3)
Coexistence	(iv)	Chronic infection equilibrium (CIE)	$\mathcal{E}_i^\dagger$	$(\overline{T}_i^\dagger, \overline{I}_i^\dagger, \overline{P}_i^\dagger, \overline{V}_i^\dagger)$	(see theorem 4 and proposition 5)
Backward bifurcation condition					$\frac{r_T}{d} > \max\left\{1 + \frac{\mu}{d}, \frac{r_P}{\mu}\right\}$ Condition Eq. (F24) holds (Theorem 6).

*Existence conditions guaranteeing the positivity of equilibria $\mathcal{E}_0^0$, $\mathcal{E}_0$, $\mathcal{E}_0^{cl}$, and $\mathcal{E}_i^\dagger$, are given in Remark 1.

3.1 Asymptotic stability of equilibria

So far, we presented conditions for the existence of equilibria. In order for the solutions of model Eq. (2) to converge to these equilibria in the long-term, we need to determine conditions for local asymptotic stability of each equilibria, given that the model's initial conditions are sufficiently close to the equilibria. In this section we will identify the parameter space that guarantees equilibria's local asymptotic stability. In general, asymptotic stability occurs

when all eigenvalues of the Jacobian matrix

$$\mathcal{J}_{(\overline{T},\overline{I},\overline{P},\overline{V})} = \begin{bmatrix} r_T - \frac{r_T(\overline{N}+\overline{T})}{K} - \beta\overline{V} - d & -\frac{r_T\overline{T}}{K} & -\frac{r_T\overline{T}}{K} + \mu & -\beta\overline{T} \\ -\frac{r_I\overline{I}}{K} + \beta\overline{V} & r_I - \frac{r_I(\overline{N}+\overline{I})}{K} - \delta - \rho & -\frac{r_I\overline{I}}{K} & \beta\overline{T} \\ -\frac{r_P\overline{P}}{K} & \rho - \frac{r_P\overline{P}}{K} & r_P - \frac{r_P(\overline{N}+\overline{P})}{K} - \mu & 0 \\ -\beta\overline{V} & \pi & 0 & -c - \beta\overline{T} \end{bmatrix} \tag{3}$$

evaluated at an equilibrium point $(\overline{T}, \overline{I}, \overline{P}, \overline{V})$ are negative or have negative real parts, where $\overline{N} = \overline{T} + \overline{I} + \overline{P}$.

Proposition 1 *The clearance with liver failure equilibrium $\mathcal{E}_0^0$ is locally asymptotically stable if $max\left\{\frac{r_T}{d}, \frac{r_I}{\delta+\rho}, \frac{r_P}{\mu}\right\} < 1$, and unstable otherwise.*

Proof See the proof in Appendix A. □

Since clearance with liver failure is not a biologically desired outcome, for the rest of the paper (unless otherwise stated) we assume that $\min\left\{\frac{r_T}{d}, \frac{r_I}{\delta+\rho}, \frac{r_P}{\mu}\right\} > 1$. Note that this is a necessary and sufficient condition for the existence of infection-free equilibrium, $\mathcal{E}_0$. Next, we derive the local stability condition for $\mathcal{E}_0$.

Let us define the basic reproduction number, $\mathcal{R}_0$, as follows:

$$\mathcal{R}_0 = \frac{r_I}{(\delta+\rho)}\left(1 - \frac{\overline{T}^0}{K}\right) + \frac{\pi}{(\delta+\rho)}\frac{\beta\overline{T}^0}{(c+\beta\overline{T}^0)}. \tag{4}$$

The threshold quantity $\mathcal{R}_0$, given by Eq. (4), gives the average number of secondary infected cells produced by one infected cell during its lifespan in a fully susceptible target cell population. The first term $\frac{r_I}{(\delta+\rho)}\left(1 - \frac{\overline{T}^0}{K}\right)$ is the average number of offspring produced by an infected cell during its lifespan (through *vertical* transmission) and the second term $\frac{\pi}{(\delta+\rho)}\frac{\beta\overline{T}^0}{(c+\beta\overline{T}^0)}$ describes the average number of secondary infections produced by one infected cell during its lifespan in a completely naive cell population (through *horizontal* transmission) [30, 29].

Theorem 2 *The infection-free equilibrium (IFE) $\mathcal{E}_0$ is locally asymptotically stable if $\mathcal{R}_0 < 1$. Otherwise, if $\mathcal{R}_0 > 1$, $\mathcal{E}_0$ is unstable.*

Proof See the proof is in Appendix B. □

Theorem 3 *Let $\overline{T}^0, \overline{I}^0, \overline{P}^0 > 0$ (see Remark 1) and assume that $\overline{P}^0 > \overline{T}^0$. If*

$$\frac{r_P}{\mu} > \frac{r_I}{\delta + \rho - \pi},$$

then the clearance with immunity equilibrium (ClImE) $\mathcal{E}_0^{cl}$ is locally asymptotically stable. Otherwise, it is unstable.

Proof See the proof in Appendix C. □

The chronic infection equilibria (CIE), $\mathcal{E}^\dagger = (\overline{T}^\dagger, \overline{I}^\dagger, \overline{P}^\dagger, \overline{V}^\dagger)$, are given by

$$\begin{aligned}
\overline{P}^\dagger &= \frac{\left[-\frac{(c+\beta\overline{T}^\dagger)d}{\beta\pi} - \frac{\overline{T}^\dagger r_T}{r_I} + \frac{(c+\beta\overline{T}^\dagger)(\rho+\delta)r_T}{\beta\pi r_I}\right]}{\left[\frac{\mu}{\rho} + \frac{\beta\overline{T}^\dagger\pi r_P}{\rho r_I(c+\beta\overline{T}^\dagger)} - \frac{(\rho+\delta)r_P}{\rho r_I} - \frac{\mu(c+\beta\overline{T}^\dagger)}{\beta\pi\overline{T}^\dagger}\right]}, \\
\overline{I}^\dagger &= \frac{r_P\overline{P}^\dagger}{\rho}\left[\frac{\beta\overline{T}^\dagger\pi}{r_I(c+\beta\overline{T}^\dagger)} + \frac{\mu}{r_P} - \frac{\rho+\delta}{r_I}\right], \\
\overline{V}^\dagger &= \frac{\pi\overline{I}^\dagger}{c+\beta\overline{T}^\dagger},
\end{aligned} \tag{5}$$

where $\overline{T}^\dagger$ is the positive root of the following quadratic polynomial:

$$P(\overline{T}^\dagger) = a_0{\overline{T}^\dagger}^4 + a_1{\overline{T}^\dagger}^3 + a_2{\overline{T}^\dagger}^2 + a_3\overline{T}^\dagger + a_4 = 0. \tag{6}$$

Detailed derivations and expressions for coefficients a_0, a_1, a_2, a_3, and a_4 are given in Appendix D. We next investigate conditions needed for the positivity of chronic infection equilibrium $\mathcal{E}^\dagger = (\overline{T}^\dagger, \overline{I}^\dagger, \overline{P}^\dagger, \overline{V}^\dagger)$.

Theorem 4 *Assume that $r_T > r_I$, $\overline{I}^0 > 0$ (see Remark 1), and*

$$max\left\{\frac{r_T}{d}, \frac{r_P}{\mu}\right\} < \frac{r_I}{\delta+\rho}. \tag{7}$$

Then equation Eq. (6) has at least one and at most three positive values of $\overline{T}^\dagger$.

Proof See the proof in Appendix D. □

Proposition 5 *Assume that $\overline{T}^\dagger > 0$ and*

$$\frac{r_I}{\delta+\rho} < \frac{r_P}{\mu}\left(1 - \frac{\beta\pi T^\dagger}{(\delta+\rho)(c+\beta T^\dagger)}\right) + \frac{r_I\rho(c+\beta T^\dagger)}{\beta\pi(\delta+\rho)T^\dagger}. \tag{8}$$

Then $I^\dagger > 0$, $V^\dagger > 0$, and $P^\dagger > 0$, ensuring the positivity of the chronic infection equilibrium (CIE) $\mathcal{E}^\dagger$ given by Eq. (5).

Proof See the proof in Appendix E. □

Next, we will show analytically and numerically that model Eq. (2) can exhibit bistable dynamics with two local attractors. Here, such bistability occurs via backward bifurcation. In the next subsection, we will derive a condition for the existence of backward bifurcation.

3.2 Bifurcation analysis

Bifurcation analysis is a powerful mathematical tool for exploring the complex behavior of mathematical models and identifying critical parameters (named bifurcation parameters) leading to transition between different outcomes [29, 30, 31, 32, 33]. Of particular interest to HBV infection is *determining biological markers responsible for the shift from clearance of the virus in some patients to development of chronic infection in others.* By determining such parameters in the modeling framework presented here (through bifurcation analysis), we aim to provide a quantitative framework for understanding the dynamics of HBV infection, suggesting potential interventions, and informing clinical decision-making to improve patient outcomes.

In this section, we prove the existence of backward and forward bifurcations in model Eq. (2) using a theorem developed by Castillo-Chavez and Song [34].

Theorem 6 *(Bifurcation at $\mathcal{R}_0 = 1$) Assume that $\frac{r_T}{d+\mu} > 1$, $\frac{r_T}{d} > \frac{r_P}{\mu}$ (alternatively, $\frac{r_T}{d} > max\left\{1 + \frac{\mu}{d}, \frac{r_P}{\mu}\right\}$), and let*

$$a = \left[\frac{2\pi\beta r_I(c+\beta\overline{T}^0)^2}{r_T} + \frac{2\beta\pi c\mu K}{r_T\overline{T}^0}\left(\frac{K\rho(c+\beta\overline{T}^0)}{r_P(\overline{T}^0-\overline{P}^0)}\right)\right]$$
$$- \left[\frac{2K\rho r_I\mu(c+\beta\overline{T}^0)^3}{r_T r_P\overline{T}^0(\overline{T}^0-\overline{P}^0)} + 2\beta\pi c\left(c+\beta\overline{T}^0 + \frac{K\rho(c+\beta\overline{T}^0)}{r_P(\overline{T}^0-\overline{P}^0)} + \frac{\pi\beta K}{r_T}\right)\right].$$

If $a > 0$, model Eq. (2) undergoes a subcritical/backward bifurcation at $\mathcal{R}_0 = 1$; namely, an unstable positive equilibrium exists for $\mathcal{R}_0$ sufficiently close to 1 from the left. If $a < 0$, model Eq. (2) undergoes a supercritical/forward bifurcation at $\mathcal{R}_0 = 1$; namely, a locally asymptotically stable positive equilibrium exists for $\mathcal{R}_0$ sufficiently close to 1 from the right.

Proof See the proof in Appendix F. □

Furthermore, for model Eq. (2), numerical simulations show that the chronic infection equilibrium (CIE) is losing stability through a Hopf bifurcation (see figure 7). We next derive the Hopf bifurcation condition analytically, by using Routh–Hurwitz Criteria. By first computing the Jacobian matrix at the CIE equilibrium $\mathcal{E}^\dagger = (\overline{T}^\dagger, \overline{I}^\dagger, \overline{P}^\dagger, \overline{V}^\dagger)$, we obtain

$$J(\mathcal{E}^\dagger) = \begin{pmatrix} -\frac{r_T\overline{T}^\dagger}{K} - \frac{\mu\overline{P}^\dagger}{T} & -\frac{r_T\overline{T}^\dagger}{K} & -\frac{r_T\overline{T}^\dagger}{K} + \mu & -\beta\overline{T}^\dagger \\ -\frac{r_I\overline{I}^\dagger}{K} + \beta\overline{V}^\dagger & r_I - \frac{r_I(\overline{T}^\dagger+2\overline{I}^\dagger+\overline{P}^\dagger)}{K} - \delta - \rho & -\frac{r_I\overline{I}^\dagger}{K} & \beta\overline{T}^\dagger \\ -\frac{r_P\overline{P}^\dagger}{K} & \rho - \frac{r_P\overline{P}^\dagger}{K} & -\frac{r_P\overline{P}^\dagger}{K} - \frac{\rho\overline{I}^\dagger}{\overline{P}^\dagger} & 0 \\ -\beta\overline{V}^\dagger & \pi & 0 & -c - \beta\overline{T}^\dagger \end{pmatrix}, \tag{9}$$

and the corresponding characteristic function

$$f(\lambda) = A_0\lambda^4 + A_1\lambda^3 + A_2\lambda^2 + A_3\lambda + A_4, \tag{10}$$

where

$$A_0 = 1, \tag{11}$$

$$A_1 = \frac{r_T\overline{T}^\dagger}{K} + \frac{\mu\overline{P}^\dagger}{\overline{T}^\dagger} - r_I + \frac{r_I(\overline{T}^\dagger + 2\overline{I}^\dagger + \overline{P}^\dagger)}{K} + \delta + \rho + \frac{r_P\overline{P}^\dagger}{K} + \frac{\rho\overline{I}^\dagger}{\overline{P}^\dagger} + c + \beta\overline{T}^\dagger, \tag{12}$$

$$\begin{aligned} A_2 = &\det\begin{pmatrix} -\frac{r_T\overline{T}^\dagger}{K} - \frac{\mu\overline{P}^\dagger}{\overline{T}^\dagger} & -\frac{r_T\overline{T}^\dagger}{K} \\ -\frac{r_I\overline{I}^\dagger}{K} + \beta\overline{V}^\dagger & r_I - \frac{r_I(\overline{T}^\dagger+2\overline{I}^\dagger+\overline{P}^\dagger)}{K} - \delta - \rho \end{pmatrix} \\ &+ \det\begin{pmatrix} -\frac{r_T\overline{T}^\dagger}{K} - \frac{\mu\overline{P}^\dagger}{\overline{T}^\dagger} & -\frac{r_T\overline{T}^\dagger}{K} + \mu \\ -\frac{r_P\overline{P}^\dagger}{K} & -\frac{r_P\overline{P}^\dagger}{K} - \frac{\rho\overline{I}^\dagger}{\overline{P}^\dagger} \end{pmatrix} + \det\begin{pmatrix} -\frac{r_T\overline{T}^\dagger}{K} - \frac{\mu\overline{P}^\dagger}{\overline{T}^\dagger} & -\beta\overline{T}^\dagger \\ -\beta\overline{V}^\dagger & -c - \beta\overline{T}^\dagger \end{pmatrix} \\ &+ \det\begin{pmatrix} r_I - \frac{r_I(\overline{T}^\dagger+2\overline{I}^\dagger+\overline{P}^\dagger)}{K} - \delta - \rho & -\frac{r_I\overline{I}^\dagger}{K} \\ \rho - \frac{r_P\overline{P}^\dagger}{K} & -\frac{\rho\overline{I}^\dagger}{\overline{P}^\dagger} - \frac{r_P\overline{P}^\dagger}{K} \end{pmatrix} \\ &+ \det\begin{pmatrix} r_I - \frac{r_I(\overline{T}^\dagger+2\overline{I}^\dagger+\overline{P}^\dagger)}{K} - \delta - \rho & \beta\overline{T}^\dagger \\ \pi & -c - \beta\overline{T}^\dagger \end{pmatrix} + \det\begin{pmatrix} -\frac{r_P\overline{P}^\dagger}{K} - \frac{\rho\overline{I}^\dagger}{\overline{P}^\dagger} & 0 \\ 0 & -c - \beta\overline{T}^\dagger \end{pmatrix}, \end{aligned} \tag{13}$$

$$\begin{aligned} A_3 = &-\det\begin{pmatrix} r_I - \frac{r_I(\overline{T}^\dagger+2\overline{I}^\dagger+\overline{P}^\dagger)}{K} - \delta - \rho & -\frac{r_I\overline{I}^\dagger}{K} & \beta\overline{T}^\dagger \\ \rho - \frac{r_P\overline{P}^\dagger}{K} & -\frac{r_P\overline{P}^\dagger}{K} - \frac{\rho\overline{I}^\dagger}{\overline{P}^\dagger} & 0 \\ \pi & 0 & -c - \beta\overline{T}^\dagger \end{pmatrix} \\ &- \det\begin{pmatrix} -\frac{r_T\overline{T}^\dagger}{K} - \frac{\mu\overline{P}^\dagger}{\overline{T}^\dagger} & -\frac{r_T\overline{T}^\dagger}{K} + \mu & -\beta\overline{T}^\dagger \\ -\frac{r_P\overline{P}^\dagger}{K} & -\frac{r_P\overline{P}^\dagger}{K} - \frac{\rho\overline{I}^\dagger}{\overline{P}^\dagger} & 0 \\ -\beta\overline{V}^\dagger & 0 & -c - \beta\overline{T}^\dagger \end{pmatrix} \end{aligned}$$

$$
\begin{aligned}
&- \det \begin{pmatrix} -\frac{r_T\overline{T}^\dagger}{K} - \frac{\mu\overline{P}^\dagger}{\overline{T}^\dagger} & -\frac{r_T\overline{T}^\dagger}{K} & -\beta\overline{T}^\dagger \\ -\frac{r_I\overline{I}^\dagger}{K} + \beta\overline{V}^\dagger & r_I - \frac{r_I(\overline{T}^\dagger+2\overline{I}^\dagger+\overline{P}^\dagger)}{K} - \delta - \rho & \beta\overline{T}^\dagger \\ -\beta\overline{V}^\dagger & \pi & -c - \beta\overline{T}^\dagger \end{pmatrix} \\
&- \det \begin{pmatrix} -\frac{r_T\overline{T}^\dagger}{K} - \frac{\mu\overline{P}^\dagger}{T} & -\frac{r_T\overline{T}^\dagger}{K} & -\frac{r_T\overline{T}^\dagger}{K} + \mu \\ -\frac{r_I\overline{I}^\dagger}{K} + \beta\overline{V}^\dagger & r_I - \frac{r_I(\overline{T}^\dagger+2\overline{I}^\dagger+\overline{P}^\dagger)}{K} - \delta - \rho & -\frac{r_I\overline{I}^\dagger}{K} \\ -\frac{r_P\overline{P}^\dagger}{K} & \rho - \frac{r_P\overline{P}^\dagger}{K} & -\frac{r_P\overline{P}^\dagger}{K} - \frac{\rho\overline{I}^\dagger}{\overline{P}^\dagger} \end{pmatrix},
\end{aligned} \tag{14}
$$

$$
A_4 = \det \begin{pmatrix} -\frac{r_T\overline{T}^\dagger}{K} - \frac{\mu\overline{P}^\dagger}{\overline{T}^\dagger} & -\frac{r_T\overline{T}^\dagger}{K} & -\frac{r_T\overline{T}^\dagger}{K} + \mu & -\beta\overline{T}^\dagger \\ -\frac{r_I\overline{I}^\dagger}{K} + \beta\overline{V}^\dagger & r_I - \frac{r_I(\overline{T}^\dagger+2\overline{I}^\dagger+\overline{P}^\dagger)}{K} - \delta - \rho & -\frac{r_I\overline{I}^\dagger}{K} & \beta\overline{T}^\dagger \\ -\frac{r_P\overline{P}^\dagger}{K} & \rho - \frac{r_P\overline{P}^\dagger}{K} & -\frac{r_P\overline{P}^\dagger}{K} - \frac{\rho\overline{I}^\dagger}{\overline{P}^\dagger} & 0 \\ -\beta\overline{V}^\dagger & \pi & 0 & -c - \beta\overline{T}^\dagger \end{pmatrix}. \tag{15}
$$

Using these coefficients, we established the result below.

Theorem 7 *(Hopf Bifurcation at a positive equilibrium) A Hopf bifurcation occurs at a positive equilibrium* $(\overline{T}^\dagger, \overline{I}^\dagger, \overline{P}^\dagger, \overline{V}^\dagger)$ *if and only if* $A_1A_2A_3 - A_1^2A_4 - A_3^2 = 0$, *where* A_0, A_1, A_2, A_3, A_4 *are defined by Eqs.* (11)-(15), *respectively.*

Proof See proof in Appendix G. □

4 Numerical simulations and bifurcation diagrams

Parameter values. We numerically investigate the parameter space where we observe different behaviors for model Eq. (2), as described in the stability analysis section. We use previously published parameters as a starting point in our simulations. Briefly, we assume that the proliferation rate for uninfected hepatocytes is $r_T = 1$ per day [25, 26, 28], for infected hepatocytes is $r_I = 0.08$ per day [23, 16], and for protected from reinfection hepatocytes is $r_P = 10^{-4}$ per day. The liver carrying capacity is $K = 1.4 \times 10^7$ hepatocyte/ mL [25, 26, 28]. The lifespan of uninfected hepatocytes was previously reported to range between 150 to 450 days [35]. We assume 150 days as the half-life of the uninfected hepatocytes, corresponding to a death rate of uninfected cells of $d = 0.005$ per day. We consider higher death rate of the infected cells, ranging between $\delta = 0.01$ and $\delta = 0.2$ per day, corresponding to infected cells lifespan between 5 and 100 days. The infectivity rate β is assumed to range between 10^{-6} and 10^{-4} mL/(virus$\times$ day), the cure rate of the infected cells to be $\rho = 10^{-3}$ per day, and the immune cell waning rate to be $\mu = 10^{-3}$ per

Table 2 Variables and parameters used in simulations

Variables	Description	Value	Reference
T	Target cells	$\overline{T}^0 = 1.4 \times 10^7$ per mL	[25, 26, 28]
I	Infected cells	$\overline{I}^0 = 0$ per mL	
P	Protected cells	$\overline{P}^0 = 0$ per mL	
V	Free virus	$\overline{V}^0$ = 1-10^9 per mL	
Parameter	Description	Value	Reference
r_T	uninfected cells proliferation rate	1 d^{-1}	[25, 26, 28]
r_I	infected cells proliferation rate	0.08 d^{-1}	[23, ?]
r_P	immune cels proliferation rate	10^{-4} d^{-1}	
K	hepatocyte carrying capacity	1.4×10^7 ml^{-1}	[25, 26, 28]
β	infectivity rate	$10^{-6} - 10^{-4}$ mL vir^{-1} d^{-1}	
d	uninfected cell death rate	0.005 d^{-1}	[23, 35]
δ	infected cell death rate	0.001 − .2 d^{-1}	
ρ	infected cell cure rate	10^{-3} d^{-1}	
μ	immune cell waning	10^{-3} d^{-1}	
π	virus production rate	0.05 d^{-1}	[23]
c	viral clearance	0.67 inf^{-1} d^{-1}	[25, 26, 28]

day. We assume a virus production rate of $\pi = 0.05$ virus/(infected cell$\times$ day) [23] and clearance rate of $c = 0.67$ per day [25, 26, 28]. A summary of these parameter values is given in Table 2.

Numerical simulations. We solve model Eq. (2) using *ODE45* in Matlab with parameters and initial conditions described above and in Table 2. Moreover, we consider two initial viral inoculum, $\overline{V}^0_{low} = 1$ virus/mL and $\overline{V}^0_{high} = 10^9$ virus/mL. As described in Section 3, model Eq. (2) has complex dynamics. Next, we will investigate model Eq. (2)'s outcomes numerically by varying the infected cells death rate δ and considering high and low initial viral loads, $\overline{V}^0_{high}$ and $\overline{V}^0_{low}$.

We find that high infected cells killing rate, $\delta = 0.12$ per day, results in virus clearance, corresponding to asymptotic stability of the infection free equilibrium (IFE), regardless of the initial viral inoculum (see Figure 2(A)-(B) and Figure 7, Region (D) and (E)). Decrease in infected cells killing rate to $\delta = 0.0845$ per day, results in bistability between the IFE and limit cycles corresponding to chronic infection equilibrium (CIE), with high viral load inoculum $\overline{V}^0_{low} = 10^9$ virus/mL resulting in convergence to a limit cycle and low viral load inoculum $\overline{V}^0_{low} = 1$ virus/mL leading to convergence to IFE (see Figure 3(A)-(B)and Figure 7, Region (C)). An even further decrease in infected cells killing rate to $\delta = 0.07$ per day, results in bistability between the IFE and the CIE, with viral inoculum deciding which equilibrium is attracting. In particular, high viral load inoculum of $\overline{V}^0_{low} = 10^9$ virus/mL results in convergence to CIE and low viral load inoculum of $\overline{V}^0_{high} = 10^9$ virus/mL results in convergence to IFE (see Figure 4(A)-(B)and Figure 7, Region (B)). To determine the transition from virus clearance to virus persistence, we plotted virus over time (see Figure 5(A) and at equilibrium (see Figure 5(B)) based on inoculum size. Numerical results suggest that with the low inoculum size ($\bar{V}^0 < 10^7$

virus/mL), virus clears and with high inoculum size ($\bar{V}^0 > 10^7$ virus/mL), virus persists. Finally, an even lower infected cells killing rate of $\delta = 0.035$ per day, results in viral persistence, corresponding to local asymptotic stability of CIE, regardless of the viral inoculum (see Figure 6 and Figure 7, Region (A)).

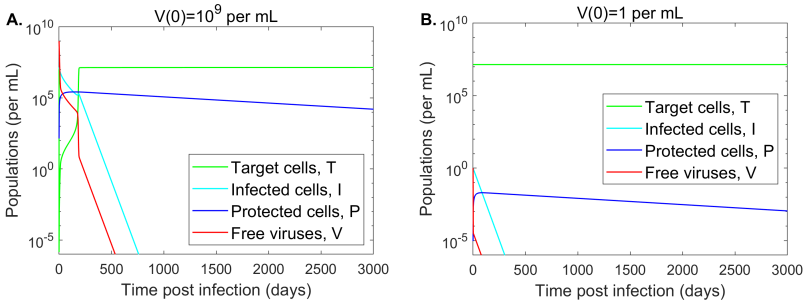

Fig. 2 Population dynamics for target cells $T(t)$ (green lines), infected cells $I(t)$ (cyan lines), protected cells $P(t)$ (blue lines), and HBV $V(t)$ (red lines) over time as given by model Eq. (2) for: (A.) $\overline{V}^0_{high} = 10^9$ virus/mL and (B.) $\overline{V}^0_{low} = 1$ virus/mL. All other parameters and initial conditions are given in Table 2. Note that this exemplifies convergence to the IFE, $\mathcal{E}_0$.

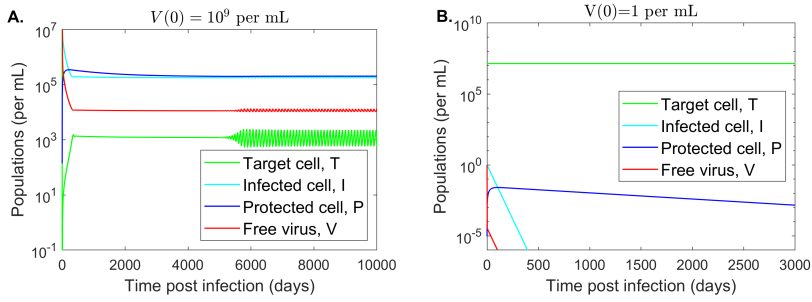

Fig. 3 Population dynamics for target cells $T(t)$ (green lines), infected cells $I(t)$ (cyan lines), protected cells $P(t)$ (blue lines), and HBV $V(t)$ (red lines) over time as given by model Eq. (2) for: (A.) $\overline{V}^0_{high} = 10^9$ virus/mL and (B.) $\overline{V}^0_{low} = 1$ virus/mL. All other parameters and initial conditions are given in Table 2. Note that this exemplifies bistability between the chronic infection equilibrium, $\mathcal{E}^\dagger$ which undergoes through Hopf bifurcation results in periodic solutions converges to limit cycles (A.) and infection-free equilibrium, $\mathcal{E}_0$ (B.).

Bifurcation analysis. An event where equilibria emerge, vanish, or alter their stability with respect to a set of parameter values, is called a bifurcation, and the curve representing changes in outcomes for a bifurcation parameter is called the bifurcation curve [36]. We next derived one-parameter (one-dimensional) bifurcation curves, with the infected cells killing rate δ as the bifurcation parameter. We consider three critical δ values: δ_c, corresponding to a *saddle node bifurcation point*; δ_h, corresponding to a *Hopf bifurcation*; and δ_0, corresponding to a *transcritical bifurcation point.*

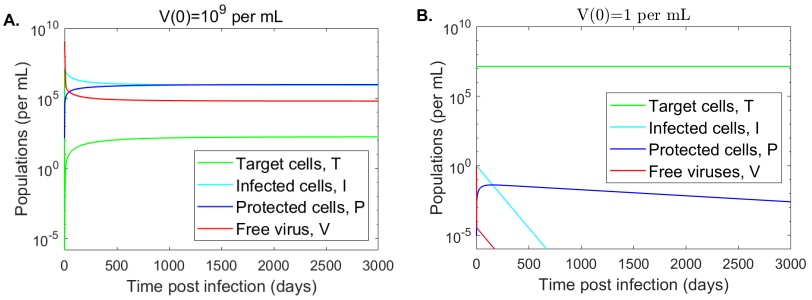

Fig. 4 Population dynamics for target cells $T(t)$ (green lines), infected cells $I(t)$ (cyan lines), protected cells $P(t)$ (blue lines), and HBV $V(t)$ (red lines) over time as given by model Eq. (2) for $\overline{V}^0_{high} = 10^9$ HBV DNA per mL (A.) and $\overline{V}^0_{low} = 1$ HBV DNA per mL (B.). All other parameters and initial conditions are given in Table 2. Note that this exemplifies bistability between the chronic infection equilibrium, $\mathcal{E}^\dagger$ (A.) and infection-free equilibrium, $\mathcal{E}_0$ (B.).

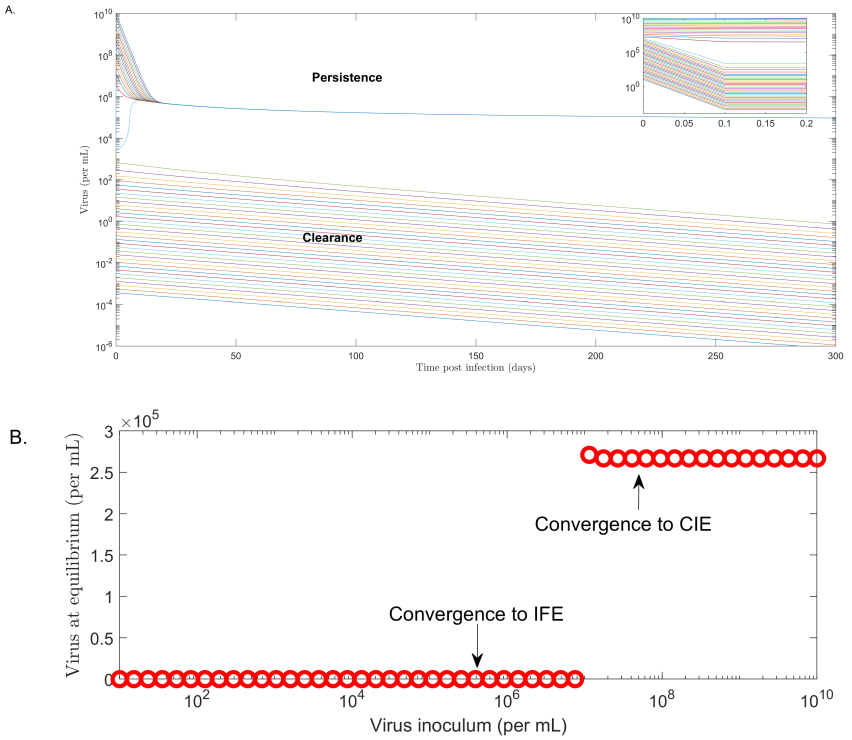

Fig. 5 Virus population $V(t)$: (A.) over time and (B.) at equilibrium as given by model Eq. (2) versus virus inoculum. Other parameters and initial conditions are given in Table 2, $\delta = 0.07$ per day, and $\beta = 10^{-4}$ mL/(virus×day). Note that $V(t)$ converges to IFE $\mathcal{E}_0$ when $\overline{V}^0 < 10^7$ virus/mL and it converges to CIE $\mathcal{E}^\dagger$ when $\overline{V}^0 > 10^7$ virus/mL.

Next, we present different bifurcation curves for the virus population at equilibrium given by model Eq. (2) for varied infected cell killing rates δ (bottom x-axis) and basic reproduction number $\mathcal{R}_0$ (top x-axis) (see Figure 7),

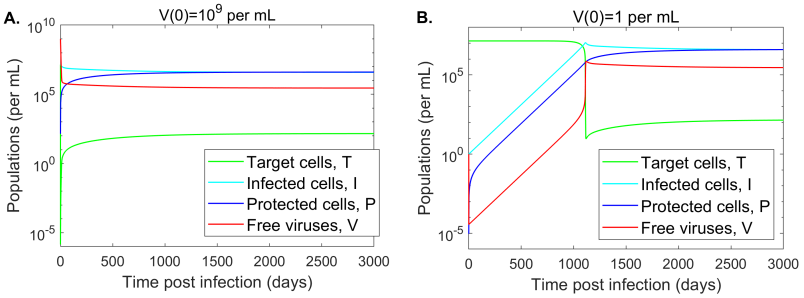

Fig. 6 Population dynamics for target cells $T(t)$ (green lines), infected cells $I(t)$ (cyan lines), protected cells $P(t)$ (blue lines), and HBV $V(t)$ (red lines) over time as given by model Eq. (2) for: (A.) $\overline{V}^0_{high} = 10^9$ virus/mL and (B.) $\overline{V}^0_{low} = 1$ virus/mL. All other parameters and initial conditions are given in Table 2. Note that this exemplifies convergence to CIE $\mathcal{E}^\dagger$.

where δ and R_0 have an inverse relationship. The first bifurcation, the *saddle node bifurcation point* δ_c, shows transition between no CIE and two CIE. In particular, there are no CIE when $\delta > \delta_c$, one CIE when $\delta = \delta_c$, and two CIE when $\delta < \delta_c$ (see Figure 7, regions D and E). Note that for all the values of δ near δ_c (from the left and right),where $\mathcal{R}_c < \mathcal{R}_0 < 1$ (here, $\mathcal{R}_c$ represents the basic reproduction number at $\delta = \delta_c$), the model (2) demonstrates that the IFE is locally asymptotically stable and virus is cleared.

The second bifurcation, the *Hopf bifurcation point* δ_h, shows emergence of limit cycles. In particular, CIE is locally asymptotically stable when $\delta < \delta_h$, CIE is unstable when $\delta > \delta_h$, and we obtain oscillatory solutions when $\delta = \delta_h$ (shaded region C in Figure 7). Note that in Figure 7, $\mathcal{R}_h$ represents the critical value of $\mathcal{R}_0$ at $\delta \in \delta_h$.

The last bifurcation, the *transcritical bifurcation point* δ_0, shows the emergence of bistable dynamics. In particular, IFE is locally asymptotically stable when $\delta < \delta_0$ ($\mathcal{R}_0 < 1$), and CIE is locally asymptotically stable and IFE is unstable when $\delta > \delta_0$ ($\mathcal{R}_0 > 1$). Furthermore, when $\mathcal{R}_0$ is sufficiently close to 1 from the right, an unstable positive CIE $\mathcal{E}^\dagger_1$ separates the basin of attraction of IFE $\mathcal{E}_0$ from that of CIE $\mathcal{E}^\dagger_2$ (see Figure 7, regions A and B). For $\mathcal{R}_0 \in [0.5913, 1]$, bistability between CIE $\mathcal{E}^\dagger_2$ and IFE $\mathcal{E}_0$ occurs via a **backward bifurcation** (see Theorem 6). Inside the bistable region, the viral inoculum size determines whether IFE $\mathcal{E}_0$ or CIE $\mathcal{E}^\dagger_2$ will be reached (see Figure 7). Hence, $\mathcal{R}_0 < 1$ is a necessary but not sufficient for viral clearance.

Bistability is a natural phenomenon, occurring via backward bifurcation (or hysteresis), and refers to dynamical systems containing multiple stable equilibria and/or limit cycles with distinct basins of attraction. In model Eq. (2), bistability occurs when the IFE and CIE are both locally asymptotically stable (see Figures 7 and Table 3). Note that model Eq. (2) has periodic solutions through Hopf bifurcation, with the CIE (inside the bistable region) losing its stability through a Hopf bifurcation and becoming unstable (see Figures 7 and Table 3).

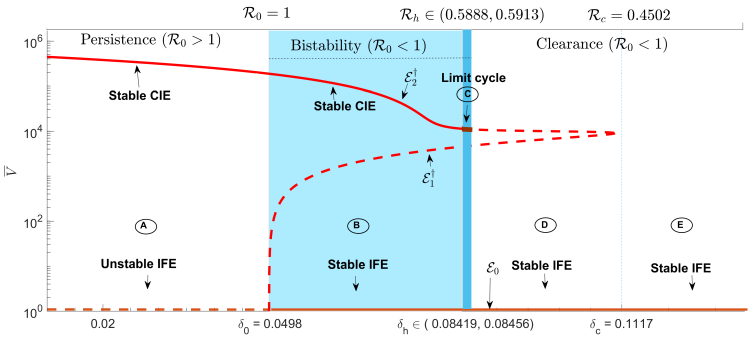

Fig. 7 Bifurcation curves for viral equilibrium as given by model Eq. (2) versus the infected cells killing rate δ (bottom x-axis) and basic reproduction number $\mathcal{R}_0$ (top x-axis). Solid, dashed, and thick solid lines represent stable, unstable, and periodic equilibria. IFE is the infection-free equilibrium ($\mathcal{E}_0$), CIE is the chronic infection equilibrium ($\mathcal{E}_1^\dagger$ and $\mathcal{E}_2^\dagger$), δ_0 is the transcritical bifurcation point, δ_h is the Hopf bifurcation point, and δ_c is the saddle node bifurcation point. All other parameters are given in Table 2.

Table 3 Summary of the one-dimensional bifurcation results from Figure 7.

Region from left to right			$\mathcal{E}_0$	$\mathcal{E}_1^\dagger$	$\mathcal{E}_2^\dagger$	system Eq. (2)
A	$\delta < \delta_0$	$\mathcal{R}_0 > 1$	US	$-^*$	LAS	converges to $\mathcal{E}_2^\dagger$
B	$\delta_0 < \delta < \delta_h$	$\mathcal{R}_h < \mathcal{R}_0 < 1$	LAS	US	LAS	shows bistability
C	$\delta \in \delta_h$	$\mathcal{R}_0 \in \mathcal{R}_h$	LAS	US	limit cycle	converges to IFE, $\mathcal{E}_0$
D	$\delta_h < \delta < \delta_c$	$\mathcal{R}_c < \mathcal{R}_0 < \mathcal{R}_h$	LAS	US	US	converges to IFE, $\mathcal{E}_0$
E	$\delta > \delta_c$	$\mathcal{R}_0 < \mathcal{R}_c$	LAS	–	–	converges to IFE, $\mathcal{E}_0$

* To represent the equilibrium does not exist, we used $-$.

For the observed dynamics above, backward bifurcation condition ($a > 0$, see theorem 6) holds. We will show numerically how we can move from backward ($a > 0$) to forward ($a < 0$) bifurcation by varying the infection rate parameter, β. Indeed if $\beta > 10^{-6}$ mL/(virus$\times$ day), we have a backward bifurcation and bistability between IFE and CIE (see Figure 8A). However, if $\beta \leq 10^{-6}$ mL/(virus$\times$ day), bistability is lost, a forward bifurcation occurs and the Hopf bifurcation region is elongated (see Figure 8B).

Lastly, we derived a two-parameter (two-dimensional) bifurcation diagram by varying the infected cells killing rate δ between 0.01 per day and 0.2 per day and the liver carrying capacity K between 10^6 hepatocytes/mL and 1.4×10^7 hepatocytes/mL, representing $7 - 100\%$ of the liver being susceptible to hepatitis B infection (see Figure 9). We find that the system displays viral persistence for low δ values, regardless of the carrying capacity K (see Figure 9, regions A and B). This means that the transcritical bifurcation occurs at the infected cell killing rate $\delta_0 = 0.04977$ per day, for all carrying capacity values K considered. As the infected cell killing rate increases, the carrying capacity influences the results. In particular, the saddle node bifurcation point changes from $\delta_c = 0.08229$ per day for $K = 10^6$ hepatocytes/mL to $\delta_c = 0.1117$ per day for $K = 1.4 \times 10^7$ hepatocytes/mL (see Figure 9, region D and E) and

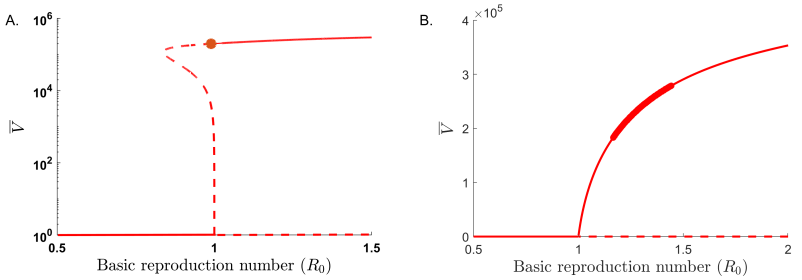

Fig. 8 Bifurcation curves for $V(t)$ at equilibrium as given by model Eq. (2) for varied basic reproduction number $\mathcal{R}_0$ values. Solid lines, dashed lines, and star represent stable, unstable, and periodic equilibria, (A.) $\beta = 2 \times 10^{-6}$ mL/(virus× day), (B.) $\beta = 1 \times 10^{-6}$ mL/(virus× day), and the rest of the parameter values are given in Table 2.

the Hopf bifurcation point varies from $\delta_h = 0.06931$ per day for $K = 10^6$ hepatocytes/mL to $\delta_h = 0.08423$ for $K = 1.4 \times 10^7$ hepatocytes/mL (see Figure 9, region C). The two-parameter bifurcation diagram shows that there is a tradeoff between target cell susceptibility to infection and host immune responses, with less infected cell killing needed for viral clearace when fewer hepatocytes are susceptible to viral infection.

Table 4 Summary of the two-dimentional bifurcation diagram results (Figure 9)

Shaded region from left to right	No. of equilibria	Stability	Outcome
A	IFE:1, CIE: 1	CIE is stable and IFE is unstable	viral persistence
B	IFE:1, CIE: 2	IFE is stable, one stable and one unstable CIE	bistablity with IFE and CIE
C	IFE:1, CIE: 2	IFE is stable, one stable and one unstable CIE	bistablity with IFE and limit cycles
D	IFE:1, CIE: 2	IFE is stable, both CIE are unstable	viral clearance
E	IFE:1, CIE: none	IFE is stable	viral clearance

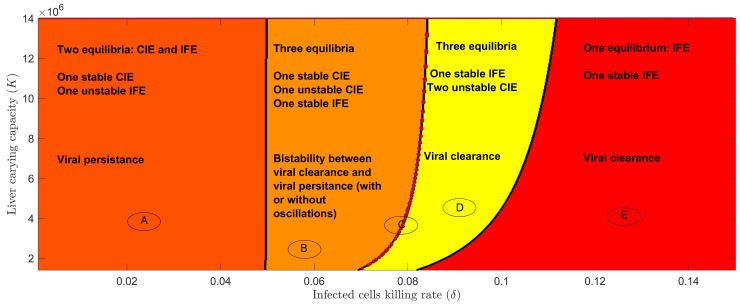

Fig. 9 Two-parameter bifurcation diagram for model Eq. (2) with varying parameters δ (killing rate of infected cells) and K (hepatocytes carrying capacity).

The basic reproduction number ($\mathcal{R}_0$) is an important threshold in epidemiology. Generally, the condition $\mathcal{R}_0 < 1$ is associated to viral clearance (i.e., the IFE is locally asymptotically stable) and the $\mathcal{R}_0 > 1$ condition is associated to viral persistence (i.e., CIE is locally asymptotically stable) (see

Figure 7). Since model Eq. (2) displays bistability, there are parameter regions where the IFE and CIE steady states are both stable when $\mathcal{R}_0 < 1$ (shaded region in Figure 7). More precisely, model Eq. (2) predicts virus clearance when $\mathcal{R}_0 < \mathcal{R}_h = 0.5913$, regardless of the size of virus inoculum. When $0.5888 = \mathcal{R}_h < \mathcal{R}_0 < 1$, however, the outcome is dependent on the size of the viral inoculum, with low inoculum dose leading to viral clearance (i.e. solutions are attracted to the IFE equilibrium) and high inoculum dose leading to viral persistence (i.e. solutions are attracted to the CIE equilibrium).

5 Discussion

We developed a mathematical model of hepatitis B infection and used it to determine the virological and immunological factors that result in viral clearance or chronic hepatitis. In previous work, we incorporated immune populations into our models, including CD8 T-cells (and their cytotoxic and non-cytotoxic functions) [26, 25, 37], antibody molecules (and their neutralizing and non-neutralizing functions) [28], as well as liver cells protected from (refractory to) reinfection [26, 38]. Here, we simplified these previous modeling assumptions by only including the population of protected liver cells, while ignoring immune populations. We did, however, include immune functions, in particular the cytotoxic CD8 T-cell immune responses (parameter δ) and non-cytotoxic CD8 T-cell immune responses (parameter ρ). A novel feature of the model is the assumption that all classes of liver cells (uninfected, infected, and protected from reinfection) proliferate at different rates. While it is well established that liver regenerates following cellular stress and death [39], the exact contribution to liver reconstitution of each of these liver classes is not understood.

We examined the model using asymptotic analyses, and found that is exhibits rich dynamics. They include parameter regions where we approach a monostable viral clearance equilibrium, parameter regions where we approach a monostable viral persistent equilibrium, and parameter regions where we have bistability of viral clearance and viral persistence equilibria.

We presented the transitions between these different outcomes in the context of three important disease markers: the basic reproduction number $\mathcal{R}_0$ (describing the expected number of infections one infected cell generates during its life span through horizontal and vertical transmission), the infected cells death rate δ (describing the effect of cytotoxic immune responses), and the liver carying capacity K (describing the liver susceptibility to infection).

We found that for low $\mathcal{R}_0$ values ($\mathcal{R}_0 < 0.5913$) virus is cleared and for high $\mathcal{R}_0$ values ($\mathcal{R}_0 > 1$) virus persists. For intermediate R_0 values ($0.5913 < \mathcal{R}_0 < 1$), however, viral clearance is dependent of viral inoculum size, with $V(0) < 10^7$ HBV/mL leading to clearance and $V(0) > 10^7$ HBV/mL leading to persistence. Bistability can occur in two ways: a parameter region where both clearance and persistent equilibria are stable (see figure 7 region (B)), and a parameter region where periodic positive solutions (through a Hopf

bifurcation) and the clearance equilibrium are bistable (see figure 7 region (C)). While the first region is biologically relevant and numerically achievable, the second region is narrow, not biologically relevant, and hard to achieve numerically.

Given that cellular immune responses (early in the infection) are crucial for viral control [40, 11, 41, 42], we described the model results through the lens of the infected cell killing rate parameter δ. We found that when $\delta > 0.08456$ per day (corresponding to an infected cell lifespan of 11.8 days, 8-times higher than the death rate of an uninfected hepatocyte), virus is cleared; when $\delta < 0.0498$ per day (corresponding to an infected cell lifespan of 20 days, 4-times higher than the death rate of an uninfected hepatocyte), virus persists, and when $\delta \in (0.0498, 0.08456)$ per day, we have bistability between clearance and persistence. In this case, clearance depends on the size of viral inoculum, with $V(0) < 10^7$ HBV/mL leading to clearance and $V(0) > 10^7$ HBV/mL leading to persistence.

Lastly, we investigated how susceptibility to hepatitis B infection affects the results, by varying the susceptible target cell population's carrying capacity parameter K, from 7% to 100% liver size. The $\delta - K$ bifurcation diagram showed that the carrying capacity K can influence the results at intermediate and high killing rates δ but has no effect when the killing rates are low (see figure 9).

Taken together, these results suggest that strong immune-mediated killing is important for viral clearance, and that the awakening of the cellular immune response is crucial to ensure viral clearance [40, 11, 41, 42]. At the intermediate killing rates, however, viral clearance can still happen depending on the size of the inoculum. Since our study investigates acute hepatitis B infection, we can relate the viral inoculum size with the routes of transmission. Hepatitis B is transmitted through sexual contact, contaminated blood (through sharing needles, syringes, and other drug-injection equipment), other body fluids, and prenatal transmission. Depending on the mode of transmission, the amount of virus inoculum establishing the infection varies, with higher levels needed for viral invasion during sexual transmission and lower levels needed for viral invasion during infected blood transmission. Therefore, the transmission route is an important heterogeneous factor that needs consideration when making personalized recommendations.

Our model has several limitations. First, we did not explicitly model the dynamics of CD8 T-cells populations. While we showed that strong cellular immune responses are needed for clearance, our model does not distinguish between immune cell population sizes and the immune potency in inducing the required response strength. Second, we ignored the dynamics of viral markers, such as serum hepatitis B surface-antigen and serum hepatitis B e-antigen, which are known to induce immune tolerance during chronic infections [43, 21, 44, 45, 46, 47]. Lastly, our results are theoretical and rely on

unknown parameters (or parameters estimated in other studies). Data validation is needed before being able to quantify the tradeoff between inoculum doses, routes of transmission, and the strength of the immune response.

In conclusion, we developed a mathematical model of hepatitis B infection and used asymptotic, bifurcation, and numerical analysis to predict the virological and immunological factors that lead to hepatitis B clearance. These results can contribute to guiding development of interventions.

Declarations

- **Funding.** HG and NA acknowledge partial support from National Science Foundation (NSF) grants DMS-1951759 and DMS-2028728. In addition HG also received partially support from NSF-NIH-NIFA Ecology and Evolution of Infectious Disease program (grant number 2208087) and NSF DMS IHBEM grant no. 2327817. Furthermore SMC acknowledges partial support from NSF grant No. 2051820 and NIH NIGMS 1R01GM152743-01. This research was enabled in part through the Virginia Tech Center for the Mathematics of Biosystems (VTCMB-033500). JMC acknowledges partial support of the NSF grant no. DMS-1714654 and National Institutes of Health, grant nos. R21-AI143443-01A1 and R01-OD011095.
- **Conflict of interest/Competing interests:** JMC has served as a consultant for Excision BioTherapeutics and Merck & Co., Inc. NA, SMC, and HG declare they have no conflict of interest. .

Appendix A

Proof of Proposition 1: We consider the local stability of the clearance with liver failure equilibrium $\mathcal{E}_0^0$. The Jacobian Eq. (3) of system Eq. (2) evaluated at $\mathcal{E}_0^0$ is

$$\mathcal{J}_{\mathcal{E}_0^0} = \begin{bmatrix} r_T - d & 0 & \mu & 0 \\ 0 & r_I - \delta - \rho & 0 & 0 \\ 0 & \rho & r_P - \mu & 0 \\ 0 & \pi & 0 & -c \end{bmatrix}.$$

The corresponding characteristic equation is given by

$$(r_T - dn - \lambda)(r_I - \delta - \rho - \lambda)(r_P - \mu - \lambda)(-c - \lambda) = 0,$$

with roots

$$\lambda_1 = r_T - d, \lambda_2 = r_I - \delta - \rho, \lambda_3 = r_P - \mu, \lambda_4 = -c.$$

$\mathcal{E}_0^0$ is locally asymptotically stable if all eigenvalues have negative real parts. This happens when

$$\frac{r_T}{d} < 1, \frac{r_I}{\delta + \rho} < 1, \text{and} \frac{r_P}{\mu} < 1.$$

That is, if $\max\left\{\frac{r_T}{d}, \frac{r_I}{\delta+\rho}, \frac{r_P}{\mu}\right\} < 1$ (alternatively, $\max\{\overline{T}^0, \overline{I}^0, \overline{P}^0\} < 0$, see Remark 1) then $\mathcal{E}_0^0$ is locally asymptotically stable, otherwise $\mathcal{E}_0^0$ is unstable. This completes the proof. □

Appendix B

Proof of Theorem 2: We linearize system Eq. (2) around the infection-free equilibrium (IFE), $\mathcal{E}_0 = (\overline{T}^0, 0, 0, 0)$ where $\overline{T}^0 = K(1 - \frac{d}{r_T})$ and $d < r_T$. The linearized subsystem can be written as $\dot{X} = (\mathcal{F} - \mathcal{V})X$ where

$$\mathcal{F} - \mathcal{V} = \begin{bmatrix} \frac{r_I d}{r_T} - \delta - \rho & \beta\overline{T}^0 \\ \pi & -c - \beta\overline{T}^0 \end{bmatrix} = \begin{bmatrix} \frac{r_I d}{r_T} & \beta\overline{T}^0 \\ 0 & 0 \end{bmatrix} - \begin{bmatrix} \delta + \rho & 0 \\ -\pi & c + \beta\overline{T}^0 \end{bmatrix}.$$

Here, entries in $\mathcal{F}$ account for new infections and entries in $\mathcal{V}$ account for movement in and out of compartments due to cell division, viral production, death, clearance or cure. We apply the next-generation matrix theory [29, 48], which states that the basic reproduction number $\mathcal{R}_0$ corresponds to the largest eigenvalue of the matrix $\mathcal{F}\mathcal{V}^{-1}$. Given that

$$\mathcal{F}\mathcal{V}^{-1} = \begin{bmatrix} \frac{r_I d}{r_T} & \beta\overline{T}^0 \\ 0 & 0 \end{bmatrix} \begin{bmatrix} \frac{1}{\delta+\rho} & 0 \\ \frac{\pi}{(\delta+\rho)(c+\beta\overline{T}^0)} & \frac{1}{c+\beta\overline{T}^0} \end{bmatrix}$$

$$= \begin{bmatrix} \frac{r_I d}{r_T(\delta+\rho)} + \frac{\pi\beta\overline{T}^0}{(\delta+\rho)(c+\beta\overline{T}^0)} & \frac{\beta\overline{T}^0}{c+\beta\overline{T}^0} \\ 0 & 0 \end{bmatrix}$$

is an upper triangular matrix, its eigenvalues are the diagonal elements. The largest eigenvalue (spectral radius) is

$$\begin{aligned} \mathcal{R}_0 &= \frac{r_I d}{r_T(\delta+\rho)} + \frac{\pi\beta\overline{T}^0}{(\delta+\rho)(c+\beta\overline{T}^0)} \\ &= \frac{r_I}{(\delta+\rho)}\frac{d}{r_T} + \frac{\pi}{(\delta+\rho)}\frac{\beta\overline{T}^0}{(c+\beta\overline{T}^0)} \\ &= \frac{r_I}{(\delta+\rho)}(1 - \frac{\overline{T}^0}{K}) + \frac{\pi}{(\delta+\rho)}\frac{\beta\overline{T}^0}{(c+\beta\overline{T}^0)}, \\ &\text{since } \overline{T}^0 = K\left(1 - \frac{d}{r_T}\right). \end{aligned}$$

This completes the proof. □

Appendix C

Proof of Theorem 3: The Jacobian matrix $\mathcal{J}$ evaluated at the clearance and immune equilibrium $\mathcal{E}_0^{cl}$ is

$$\mathcal{J}_{\mathcal{E}_0^{cl}} = \begin{bmatrix} r_T\left(\frac{\mu}{r_P} - \frac{d}{r_T}\right) - \frac{r_T\overline{T}^*}{K} & -\frac{r_T\overline{T}^*}{K} & -\frac{r_T\overline{T}^*}{K} + \mu & -\beta\overline{T}^* \\ 0 & r_I\left(\frac{\mu}{r_P} - \frac{\delta+\rho}{r_I}\right) & 0 & \beta\overline{T}^* \\ -\frac{r_P\overline{P}^*}{K} & \rho - \frac{r_P\overline{P}^*}{K} & -\frac{r_P\overline{P}^*}{K} & 0 \\ 0 & \pi & 0 & -c - \beta\overline{T}^* \end{bmatrix}$$

$$= \begin{bmatrix} -\frac{r_T}{K}(\overline{P}^0 - \overline{T}^0) - \frac{r_T\overline{T}^*}{K} & -\frac{r_T\overline{T}^*}{K} & -\frac{r_T\overline{T}^*}{K} + \mu & -\beta\overline{T}^* \\ 0 & -\frac{r_I}{K}(\overline{P}^0 - \overline{I}^0) & 0 & \beta\overline{T}^* \\ -\frac{r_P\overline{P}^*}{K} & \rho - \frac{r_P\overline{P}^*}{K} & -\frac{r_P\overline{P}^*}{K} & 0 \\ 0 & \pi & 0 & -c - \beta\overline{T}^* \end{bmatrix}.$$

The corresponding characteristic polynomial is given by

$$f(\lambda) = a_0\lambda^4 + a_1\lambda^3 + a_2\lambda^2 + a_3\lambda + a_4, \tag{C1}$$

where

$$a_0 = 1,$$

$$a_1 = \frac{r_T}{K}(\overline{P}^0 - \overline{T}^0) + \frac{r_I}{K}(\overline{P}^0 - \overline{I}^0) + \frac{r_P\overline{P}^*}{K} + \frac{r_T\overline{T}^*}{K} + c + \beta\overline{T}^*,$$

$$a_2 = \frac{r_P\overline{P}^*}{K}\left(\frac{r_T}{K}(\overline{P}^0 - \overline{T}^0) + \mu\right) + \frac{r_I c}{K}(\overline{P}^0 - \overline{I}^0) + \beta\overline{T}^*\left(\frac{r_I}{K}(\overline{P}^0 - \overline{I}^0) - \pi\right)$$
$$+ \left(\frac{r_I}{K}(\overline{P}^0 - \overline{I}^0) + c + \beta\overline{T}^*\right)\left(\frac{r_T}{K}(\overline{P}^0 - \overline{T}^0) + \frac{r_P\overline{P}^*}{K} + \frac{r_T\overline{T}^*}{K}\right),$$

$$a_3 = \frac{r_P\overline{P}^*}{K}\left(\frac{r_I}{K}(\overline{P}^0 - \overline{I}^0) + c + \beta\overline{T}^*\right)\left(\frac{r_T}{K}(\overline{P}^0 - \overline{T}^0) + \mu\right)$$
$$+ \left(\frac{r_T}{K}(\overline{P}^0 - \overline{T}^0) + \frac{r_P\overline{P}^*}{K} + \frac{r_T\overline{T}^*}{K}\right)\left(\frac{r_I c}{K}(\overline{P}^0 - \overline{I}^0) + \beta\overline{T}^*\left(\frac{r_I}{K}(\overline{P}^0 - \overline{I}^0) - \pi\right)\right),$$

$$a_4 = \frac{r_P\overline{P}^*}{K}\left(\frac{r_T}{K}(\overline{P}^0 - \overline{T}^0) + \mu\right)\left(\frac{r_I c}{K}(\overline{P}^0 - \overline{I}^0) + \beta\overline{T}^*\left(\frac{r_I}{K}(\overline{P}^0 - \overline{I}^0) - \pi\right)\right),$$

where $\overline{T}^0 = K(1 - \frac{d}{r_T})$, $\overline{I}^0 = K(1 - \frac{\delta+\rho}{r_I})$, and $\overline{P}^0 = K(1 - \frac{\mu}{r_P})$.

Note that if

$$\overline{P}^0 > \overline{I}^0 + \frac{\pi K}{r_I} \Longleftrightarrow \frac{r_P}{\mu} > \frac{r_I}{\delta + \rho - \pi}, \tag{C2}$$

then $a_i > 0,\ i = \{0, ..., 4\}$. To establish the asymptotic stability of the $\mathcal{E}_0^{cl}$ equilibrium, we are using the Routh-Hurwitz criterion. The Hurwitz matrices are

$$H_1 = [a_1] \tag{C3}$$

$$H_2 = \begin{bmatrix} a_1 & 1 \\ a_3 & a_2 \end{bmatrix} \tag{C4}$$

$$H_3 = \begin{bmatrix} a_1 & 1 & 0 \\ a_3 & a_2 & a_1 \\ 0 & a_4 & a_3 \end{bmatrix} \tag{C5}$$

$$H_4 = \begin{bmatrix} a_1 & 1 & 0 & 0 \\ a_3 & a_2 & a_1 & 1 \\ 0 & a_4 & a_3 & a_2 \\ 0 & 0 & 0 & a_4 \end{bmatrix}. \tag{C6}$$

According to the Routh-Hurwitz stability criterion a fourth-order system has eigenvalues with negative real parts if and only if the Hurwitz matrices have positive determinants, that is $det(H_i) > 0,\ i = \{0, ..., 4\}$.
For simplicity, let

$$b_1 = \frac{r_T}{K}(\overline{P}^0 - \overline{T}^0) + \frac{r_P\overline{P}^*}{K} + \frac{r_T\overline{T}^*}{K},$$
$$b_2 = \frac{r_I}{K}(\overline{P}^0 - \overline{I}^0) + c + \beta\overline{T}^*,$$
$$b_3 = \frac{r_P\overline{P}^*}{K}\left(\frac{r_T}{K}(\overline{P}^0 - \overline{T}^0) + \mu\right),$$

$$b_4 = \frac{r_I c}{K}(\overline{P}^0 - \overline{I}^0) + \beta\overline{T}^* \left(\frac{r_I}{K}(\overline{P}^0 - \overline{I}^0) - \pi\right).$$

which implies $a_1 = b_1 + b_2, a_2 = b_1b_2 + b_3 + b_4, a_3 = b_1b_4 + b_2b_3$ and $a_4 = b_3b_4$. Notice b_1, b_2, b_3, b_4 are positive when condition (C2) holds. Hurwitz matrices become $H_1 = b_1 + b_2, H_2 = b_1b_3 + b_2b_4 + b_1b_2(b_1 + b_2), H_3 = b_1b_2(b_3 - b_4)^2 + b_1b_2(b_1 + b_2)(b_1b_4 + b_2b_3), H_4 = a_4H_3$, which shows that the Hurwitz determinants are positive if condition Eq. (C2) holds. This completes the proof. □

Appendix D

Proof of Theorem 4: Let, $\mathcal{E}^\dagger = (\overline{T}^\dagger, \overline{I}^\dagger, \overline{P}^\dagger, \overline{V}^\dagger)$ denote the chronic infection equilibria (CIE) of system Eq. (2) with all variables in the positive orthant. Setting the right-hand side of the system Eq. (2) equal to zero results in the following conditions

$$\overline{V}^\dagger = \frac{\pi\overline{I}^\dagger}{c + \beta\overline{T}^\dagger}, \tag{D7}$$

$$1 - \frac{N^\dagger}{K} = \frac{\beta\pi\overline{I}^\dagger}{r_T(c + \beta\overline{T}^\dagger)} + \frac{d}{r_T} - \frac{\mu\overline{P}^\dagger}{r_T\overline{T}^\dagger}, \tag{D8}$$

$$1 - \frac{N^\dagger}{K} = \frac{-\beta\overline{T}^\dagger\pi}{r_I(c + \beta\overline{T}^\dagger)} + \frac{\rho + \delta}{r_I}, \tag{D9}$$

and

$$1 - \frac{N^\dagger}{K} = \frac{-\rho\overline{I}^\dagger}{r_P\overline{P}^\dagger} + \frac{\mu}{r_P}, \tag{D10}$$

where $N^\dagger = \overline{T}^\dagger + \overline{I}^\dagger + \overline{P}^\dagger$. From Eq. (D8) and Eq. (D9) we obtain

$$\overline{I}^\dagger = \frac{r_T(c + \beta\overline{T}^\dagger)}{\beta\pi}\left[\frac{\mu\overline{P}^\dagger}{r_T\overline{T}^\dagger} - \frac{\beta\overline{T}^\dagger\pi}{r_I(c + \beta\overline{T}^\dagger)} + \frac{\rho + \delta}{r_I} - \frac{d}{r_T}\right]. \tag{D11}$$

From Eq. (D9) and Eq. (D10), we obtain

$$\overline{I}^\dagger = \frac{r_P\overline{P}^\dagger}{\rho}\left[\frac{\beta\overline{T}^\dagger\pi}{r_I(c + \beta\overline{T}^\dagger)} + \frac{\mu}{r_P} - \frac{\rho + \delta}{r_I}\right] \tag{D12}$$

Lastly, from Eq. (D11) and Eq. (D12), we obtain

$$\overline{P}^\dagger = \frac{\left[-\frac{(c+\beta\overline{T}^\dagger)d}{\beta\pi} - \frac{\overline{T}^\dagger r_T}{r_I} + \frac{(c+\beta\overline{T}^\dagger)(\rho+\delta)r_T}{\beta\pi r_I}\right]}{\left[\frac{\mu}{\rho} + \frac{\beta\overline{T}^\dagger\pi r_P}{\rho r_I(c+\beta\overline{T}^\dagger)} - \frac{(\rho+\delta)r_P}{\rho r_I} - \frac{\mu(c+\beta\overline{T}^\dagger)}{\beta\pi\overline{T}^\dagger}\right]}. \tag{D13}$$

Substituting Eq. (D13) into Eq. (D12) leads to

$$\overline{I}^\dagger = \frac{\left[-\frac{(c+\beta\overline{T}^\dagger)d}{\beta\pi} - \frac{\overline{T}^\dagger r_T}{r_I} + \frac{(c+\beta\overline{T}^\dagger)(\rho+\delta)r_T}{\beta\pi r_I}\right]\left[\frac{\mu}{\rho} + \frac{\beta\overline{T}^\dagger\pi r_P}{\rho r_I(c+\beta\overline{T}^\dagger)} - \frac{(\rho+\delta)r_P}{\rho r_I}\right]}{\left[\frac{\mu}{\rho} + \frac{\beta\overline{T}^\dagger\pi r_P}{\rho r_I(c+\beta\overline{T}^\dagger)} - \frac{(\rho+\delta)r_P}{\rho r_I} - \frac{\mu(c+\beta\overline{T}^\dagger)}{\beta\pi\overline{T}^\dagger}\right]}, \tag{D14}$$

and substituting Eq. (D14) into Eq. (D7) leads to

$$\overline{V}^{\dagger} = \frac{\pi\left[-\frac{d(c+\beta\overline{T}^{\dagger})}{\beta\pi} - \frac{\overline{T}^{\dagger}r_T}{r_I} + \frac{(c+\beta\overline{T}^{\dagger})(\rho+\delta)r_T}{\beta\pi r_I}\right]\left[\frac{\mu}{\rho} + \frac{\beta\overline{T}^{\dagger}\pi r_P}{\rho r_I(c+\beta\overline{T}^{\dagger})} - \frac{(\rho+\delta)r_P}{\rho r_I}\right]}{(c+\beta\overline{T}^{\dagger})\left[\frac{\mu}{\rho} + \frac{\beta\overline{T}^{\dagger}\pi r_P}{\rho r_I(c+\beta\overline{T}^{\dagger})} - \frac{(\rho+\delta)r_P}{\rho r_I} - \frac{\mu(c+\beta\overline{T}^{\dagger})}{\beta\pi\overline{T}^{\dagger}}\right]}. \tag{D15}$$

Substituting Eq. (D13), Eq. (D14) and Eq. (D15) into the target cell equation of system Eq. (2), results in the quartic polynomial in $\overline{T}^{\dagger}$ given as

$$P(\overline{T}^{\dagger}) = a_0{\overline{T}^{\dagger}}^4 + a_1{\overline{T}^{\dagger}}^3 + a_2{\overline{T}^{\dagger}}^2 + a_3\overline{T}^{\dagger} + a_4.$$

Its coefficients are

$$\begin{aligned}
a_0 &= \frac{\beta^2 r_T}{Kr_I}\left[\frac{\pi r_P}{\rho}\left(\frac{r_T}{r_I}-1\right) + r_T + \frac{\mu r_I}{\pi} + \frac{\mu(\delta+\rho)}{\rho}\left(\frac{r_I}{\delta+\rho} - \frac{r_P}{\mu}\right)\left(\frac{r_T}{r_I}-1\right)\right.\\
&\left. + d(\delta+\rho)\left(\frac{r_P}{\rho r_I} + \frac{1}{\pi}\right)\left(\frac{r_I}{\delta+\rho} - \frac{r_T}{d}\right) + \frac{d\mu(\delta+\rho)^2}{\pi\rho r_I}\left(\frac{r_I}{\delta+\rho} - \frac{r_T}{d}\right)\left(\frac{r_I}{\delta+\rho} - \frac{r_P}{\mu}\right)\right],\\
a_1 &= \frac{\pi\beta r_T}{K\rho r_I}\left[\frac{c}{\pi}\left(\frac{r_T}{r_I}-1\right)\left(\pi r_P + 2\mu(\delta+\rho)\left(\frac{r_I}{\delta+\rho} - \frac{r_P}{\mu}\right)\right)\right.\\
&+ \frac{K\beta\pi r_P}{r_I} + \frac{K\beta\mu(\delta+\rho)}{r_I}\left(\frac{r_I}{\delta+\rho}-1\right)\left(\frac{r_P}{\mu} - \frac{\rho r_I}{\pi^2}\right)\\
&+ \frac{2cr_T\rho}{\pi} + \frac{cd(\delta+\rho)}{\pi^2}\left(\frac{r_I}{\delta+\rho} - \frac{r_T}{d}\right)\left(3\rho + \frac{2r_P\pi}{r_I} + \frac{3\mu(\delta+\rho)}{r_I}\left(\frac{r_I}{\delta+\rho} - \frac{r_P}{\mu}\right)\right)\\
&\left. + \frac{K\beta\mu(\delta+\rho)}{\pi r_I}\left(\frac{r_I}{\delta+\rho} - \frac{r_P}{\mu}\right)\left(\pi + (\delta+\rho)\left(\frac{r_I}{\delta+\rho}-1\right)\right) - \frac{K\beta\rho\mu}{\pi} + \frac{3c\rho\mu r_I}{\pi^2}\right],\\
a_2 &= \frac{cr_T(\delta+\rho)}{r_I}\left(\frac{r_I}{\delta+\rho}-1\right)\left(\frac{\beta\pi r_P}{\rho r_I} + \frac{2\beta\mu(\delta+\rho)}{\rho r_I}\left(\frac{r_I}{\delta+\rho} - \frac{r_P}{\mu}\right) - \frac{3\beta\mu}{\pi}\right)\\
&+ \frac{c\mu}{K\rho}\left(\frac{r_T}{r_I}-1\right)\left(\frac{r_I}{\delta+\rho} - \frac{r_P}{\mu}\right) + \frac{cd}{K}\left(\frac{r_I}{\delta+\rho} - \frac{r_T}{d}\right)\left(\frac{r_P}{\rho r_I} + \frac{3}{\pi}\right)\\
&+ \left(\frac{r_I}{\delta+\rho} - \frac{r_P}{\mu}\right)\left(\frac{\beta\pi\mu}{\rho r_I} + \frac{3cd\mu(\delta+\rho)}{K\pi\rho r_I}\left(\frac{r_I}{\delta+\rho} - \frac{r_T}{d}\right)\right) + \frac{cr_T}{K(\delta+\rho)}\\
&- \frac{2\beta\mu}{\delta+\rho} + \frac{3c\mu r_I}{Kp(\delta+\rho)},\\
a_3 &= \frac{c^2 r_T\mu}{\rho r_I}\left[\left(1 - \frac{\delta+\rho}{r_I}\right)\left\{(\delta+\rho)\left(\frac{r_I}{\delta+\rho} - \frac{r_P}{\mu}\right) - \frac{3\rho r_I}{\pi}\right\} - \rho\right]\\
&+ \frac{c^3 r_T}{K\beta\pi}\left[\left(\frac{r_I}{\delta+\rho} - \frac{r_T}{d}\right)\left\{\frac{d(\delta+\rho)^2\mu}{\rho r_I^2}\left(\frac{r_I}{\delta+\rho} - \frac{r_P}{\mu}\right) + \frac{d(\delta+\rho)}{r_I}\right\} + \mu\right],\\
a_4 &= -\frac{c^3\mu r_T}{\pi}\left(1 - \frac{\delta+\rho}{r_I}\right) = -\frac{c^3\mu r_T\overline{I}^0}{\pi K}.
\end{aligned}$$

If $\frac{r_T}{r_I} > 1$ and $\max\left\{\frac{r_T}{d}, \frac{r_P}{\mu}\right\} < \frac{r_I}{\delta+\rho}$ (i.e., $\max\{\overline{T}^0, \overline{P}^0\} < \overline{I}^0$), then a_0 is positive. Moreover, if $\frac{r_I}{\delta+\rho} > 1$ (i.e., $\overline{I}^0 > 0$), then a_4 is negative. When $a_0 > 0$ and $a_4 < 0$, the number of possible positive roots for equation Eq. (6) depends on the signs of the remaining coefficients a_1, a_2, and a_3. This can be analyzed by using the Descarte's rule of sign on the quartic polynomial function $P(T^{\dagger})$ defined in equation

Table D1 Number of possible positive real roots of $P(T^\dagger)$

Cases	a_0	a_1	a_2	a_3	a_4	No. of sign changes	No. of positive real roots
1	+	+	+	+	−	1	1
2	+	+	+	−	−	1	1
3	+	+	−	+	−	3	3
4	+	−	+	−	−	3	3
5	+	−	−	−	−	1	1
6	+	−	−	+	−	3	3
7	+	−	+	−	−	3	3
8	+	+	−	−	−	1	1

Eq. (6). The different possibilities for the roots $P(T^\dagger)$ are tabulated in Table(D1). Hence, equation Eq. (6) has one positive root when cases 1, 2, 5, and 8 in Table(D1) are satisfied and three positive roots when cases 3, 4, 6, and 7 in Table(D1) are satisfied. This completes the proof. □

Appendix E

Proof of Proposition 5: Assuming that $\overline{T}^\dagger > 0$, we obtain that $\overline{P}^\dagger > 0$ and $\overline{I}^\dagger > 0$ when

$$\frac{r_T}{d}\left(1 - \frac{\beta\pi T^\dagger}{(\delta+\rho)(c+\beta T^\dagger)}\right) < \frac{r_I}{\delta+\rho} < \frac{r_P}{\mu}\left(1 - \frac{\beta\pi T^\dagger}{(\delta+\rho)(c+\beta T^\dagger)}\right) + \frac{r_I\rho(c+\beta T^\dagger)}{\beta\pi(\delta+\rho)T^\dagger}, \tag{E16}$$

and

$$\frac{r_I}{\delta+\rho} < \frac{r_P}{\mu}\left(1 - \frac{\beta\pi T^\dagger}{(\delta+\rho)(c+\beta T^\dagger)}\right). \tag{E17}$$

Moreover, $\overline{V}^\dagger > 0$ when $\overline{I}^\dagger > 0$. Combining Eq. (E16) and Eq. (E17) and using the fact that

$$\max\left\{\frac{r_T}{d}\left(1 - \frac{\beta\pi T^\dagger}{(\delta+\rho)(c+\beta T^\dagger)}\right), \frac{r_P}{\mu}\left(1 - \frac{\beta\pi T^\dagger}{(\delta+\rho)(c+\beta T^\dagger)}\right)\right\} < \max\left\{\frac{r_T}{d}, \frac{r_P}{\mu}\right\}$$

we get

$$\max\left\{\frac{r_T}{d}, \frac{r_P}{\mu}\right\} < \frac{r_I}{\delta+\rho} < \frac{r_P}{\mu}\left(1 - \frac{\beta\pi T^\dagger}{(\delta+\rho)(c+\beta T^\dagger)}\right) + \frac{r_I\rho(c+\beta T^\dagger)}{\beta\pi(\delta+\rho)T^\dagger}.$$

Note that $\overline{T}^\dagger$ is positive then

$$\frac{r_I}{\delta+\rho} < \frac{r_P}{\mu}\left(1 - \frac{\beta\pi T^\dagger}{(\delta+\rho)(c+\beta T^\dagger)}\right) + \frac{r_I\rho(c+\beta T^\dagger)}{\beta\pi(\delta+\rho)T^\dagger},$$

which completes the proof. □

Appendix F

Proof of Theorem 6: In this section, we prove the backward bifurcation condition using the center manifold theory [49]. We choose the infected clearance rate (δ) as the bifurcation parameter, solve $\mathcal{R}_0 = 1$, and obtain the following critical value (δ_0)

$$\delta_0 = \frac{r_I d}{r_T} + \frac{\pi\beta\overline{T}^0}{c+\beta\overline{T}^0} - \rho. \tag{F18}$$

To apply the center manifold theory, let us first change the variables of system Eq. (2) to $X = (x_1, x_2, x_3, x_4)$, where $x_1 = T$, $x_2 = I$, $x_3 = P$, and $x_4 = V$. Moreover, we assume all but parameter δ are known. Then, model Eq. (2) becomes

$$\frac{\mathrm{d}X}{\mathrm{d}t} = f(X, \delta),$$

where

$$f \in C^2(R^4 \times R, R^4)$$

is given by

$$\begin{aligned}
\frac{dx_1}{dt} &= f_1 = r_T\, x_1 \left(1 - \frac{x_1 + x_2 + x_3}{K}\right) - \beta x_1 x_4 + \mu x_3 - d x_1,\\
\frac{dx_2}{dt} &= f_2 = r_I\, x_2 \left(1 - \frac{x_1 + x_2 + x_3}{K}\right) + \beta x_1 x_4 - \delta x_2 - \rho x_2,\\
\frac{dx_3}{dt} &= f_3 = r_R\, x_3 \left(1 - \frac{x_1 + x_2 + x_3}{K}\right) - \mu x_3 + \rho x_2,\\
\frac{dx_4}{dt} &= f_4 = \pi x_2 - c x_4 - \beta x_1 x_4.
\end{aligned}$$

Let $J_{\delta_0}(\mathcal{E}_0)$ denote the Jacobian of system Eq. (2) evaluated at the infection free equilibrium ($\mathcal{E}_0$) for the critical parameter $\delta = \delta_0$

$$J_{\delta_0}(\mathcal{E}_0) = \begin{bmatrix} d - r_T & d - r_T & d - r_T + \mu & -\beta\overline{T}^0 \\ 0 & -\frac{p\beta\overline{T}^0}{c+\beta\overline{T}^0} & 0 & \beta\overline{T}^0 \\ 0 & \rho & \frac{dr_P}{r_T} - \mu & 0 \\ 0 & \pi & 0 & -c - \beta\overline{T}^0 \end{bmatrix}. \tag{F19}$$

Then, the characteristic polynomial of $J_{\delta_0}(\mathcal{E}_0)$ is

$$f(\lambda) = \lambda\,(d - r_T - \lambda)\left(\frac{dr_P}{r_T} - \mu - \lambda\right)\left(\lambda + c + \beta\overline{T}^0 + \frac{\pi\beta\overline{T}^0}{c + \beta\overline{T}^0}\right). \tag{F20}$$

Assume that $\overline{T}^0 > 0$ (i.e., $\frac{r_T}{d} > 1$) and $\overline{T}^0 > \overline{P}^0$ (i.e., $\frac{r_T}{d} > \frac{r_P}{\mu}$), then system Eq. (2), with $\delta = \delta_0$, exhibits a non-hyperbolic equilibrium point (i.e., the linearized system Eq. (F19) has a simple eigenvalue with zero real part and all other eigenvalues have negative real part).

If $\mathcal{R}_0 = 1$, it can be shown that $J_{\delta_0}(\mathcal{E}_0)$ has a left(row) eigenvector, $\mathbf{v} = [v_1, v_2, v_3, v_4]$, corresponding to the 0 eigenvalue and given by

$$v_1 = 0, v_2 = c + \beta\overline{T}^0, v_3 = 0, v_4 = \beta\overline{T}^0, \tag{F21}$$

where all v_i are non-negative. Similarly, $J_{\delta_0}(\mathcal{E}_0)$ has a right(column) eigenvector, $\mathbf{w} = [w_1, w_2, w_3, w_4]^T$, corresponding to the 0 eigenvalue and given by

$$\begin{aligned}
w_1 &= -\frac{\pi\beta\overline{T}^0}{r_T - d} - (c + \beta\overline{T}^0) - \frac{r_T - d - \mu}{r_T - d}\left(\frac{K\rho(c + \beta\overline{T}^0)}{r_P(\overline{T}^0 - \overline{P}^0)}\right),\\
w_2 &= c + \beta\overline{T}^0,\\
w_3 &= \frac{K\rho(c + \beta\overline{T}^0)}{r_P(\overline{T}^0 - \overline{P}^0)},\\
w_4 &= \pi.
\end{aligned} \tag{F22}$$

Note that, $\overline{T}^0 > \frac{K\mu}{r_T}$ if and only if $r_T > d+\mu$. Moreover, $w_1 < 0,\ w_2 > 0,\ w_3 > 0,$ and $w_4 > 0$. We used Theorem 4.1 [34] to establish the existence of a backward bifurcation for Eq. (2). The local bifurcation analysis near the bifurcation point $(\delta = \delta_0)$ is then determined by the sign of two associated constants, denoted by a and b defined (respectively) by

$$a = \sum_{i,j,k=1}^{4} v_k w_i w_j \frac{\partial^2 f_k(0,0)}{\partial x_i \partial x_j} \quad \text{and} \quad b = \sum_{i,k=1}^{4} v_k w_i \frac{\partial^2 f_k(0,0)}{\partial x_i \partial \phi},$$

with $\phi = \delta - \delta_0$. It is worth noting that, in $f_k(0,0)$ the first zero corresponds to the IFE, $\mathcal{E}_0$, for the system Eq. (2). In other words, $f_k(0,\phi) = 0$, for $k = \{1,...,4\}$ if and only if the right-hand side of all equations in system Eq. (2) are zero at $\mathcal{E}_0$. Moreover since $(\delta = \delta_0)$ is the bifurcation parameter, it follows from $\phi = \delta - \delta_0$ that $\phi = 0$ when $\delta = \delta_0$, which is the second component of $f_k(0,0)$.

Computation of a: To compute a, we need to find the following partial derivatives

$$\frac{\partial^2 f_2}{\partial x_1^2} = 0,\ \frac{\partial^2 f_2}{\partial x_1 \partial x_2} = -\frac{r_I}{K},\ \frac{\partial^2 f_2}{\partial x_1 \partial x_3} = 0,\ \frac{\partial^2 f_2}{\partial x_1 \partial x_4} = \beta,$$

$$\frac{\partial^2 f_2}{\partial x_2 \partial x_1} = -\frac{r_I}{K}, \frac{\partial^2 f_2}{\partial x_2^2} = -\frac{2r_I}{K},\ \frac{\partial^2 f_2}{\partial x_2 \partial x_3} = -\frac{r_I}{K},\ \frac{\partial^2 f_2}{\partial x_2 \partial x_4} = 0,$$

$$\frac{\partial^2 f_2}{\partial x_3 \partial x_1} = 0, \frac{\partial^2 f_2}{\partial x_3 \partial x_2} = -\frac{r_I}{K},\ \frac{\partial^2 f_2}{\partial x_3^2} = 0,\ \frac{\partial^2 f_2}{\partial x_3 \partial x_4} = 0,$$

$$\frac{\partial^2 f_2}{\partial x_4 \partial x_1} = \beta, \frac{\partial^2 f_2}{\partial x_4 \partial x_2} = 0,\ \frac{\partial^2 f_2}{\partial x_4 \partial x_3} = 0,\ \frac{\partial^2 f_2}{\partial x_4^2} = 0,$$

$$\frac{\partial^2 f_4}{\partial x_1^2} = 0,\ \frac{\partial^2 f_4}{\partial x_1 \partial x_2} = 0,\ \frac{\partial^2 f_4}{\partial x_1 \partial x_3} = 0,\ \frac{\partial^2 f_4}{\partial x_1 \partial x_4} = -\beta,$$

$$\frac{\partial^2 f_4}{\partial x_2 \partial x_1} = 0, \frac{\partial^2 f_4}{\partial x_2^2} = 0,\ \frac{\partial^2 f_4}{\partial x_2 \partial x_3} = 0,\ \frac{\partial^2 f_4}{\partial x_2 \partial x_4} = 0,$$

$$\frac{\partial^2 f_4}{\partial x_3 \partial x_1} = 0, \frac{\partial^2 f_4}{\partial x_3 \partial x_2} = 0,\ \frac{\partial^2 f_4}{\partial x_3^2} = 0,\ \frac{\partial^2 f_4}{\partial x_3 \partial x_4} = 0,$$

$$\frac{\partial^2 f_4}{\partial x_4 \partial x_1} = -\beta, \frac{\partial^2 f_4}{\partial x_4 \partial x_2} = 0,\ \frac{\partial^2 f_4}{\partial x_4 \partial x_3} = 0,\ \frac{\partial^2 f_4}{\partial x_4^2} = 0,$$

Substituting vectors $\mathbf{v}$ defined in equation(F21) and $\mathbf{w}$ defined in equation(F22) into the partial derivatives (evaluated at the IFE $\mathcal{E}_0$) simplifies to

$$a = \sum_{i,j,k=1}^{4} v_k w_i w_j \frac{\partial^2 f_k(0,0)}{\partial x_i \partial x_j}.$$

After some algebraic manipulation this becomes

$$a = 2\beta w_1 w_4 (v_2 - v_4) - \frac{2r_I w_2 v_2 (w_1 + w_2 + w_3)}{K}.$$

Using the values of w_1, w_2, w_3, w_4, v_2, and v_4

$$a = \left[\frac{2\pi\beta r_I (c + \beta\overline{T}^0)^2}{r_T} + \frac{2\beta\pi c\mu K}{r_T \overline{T}^0} \left(\frac{K\rho(c + \beta\overline{T}^0)}{r_P(\overline{T}^0 - \overline{P}^0)} \right) \right]$$

$$- \left[\frac{2K\rho r_I \mu (c+\beta\overline{T}^0)^3}{r_T r_P \overline{T}^0 (\overline{T}^0 - \overline{P}^0)} + 2\beta\pi c \left(c + \beta\overline{T}^0 + \frac{K\rho(c+\beta\overline{T}^0)}{r_P(\overline{T}^0 - \overline{P}^0)} + \frac{\pi\beta K}{r_T} \right) \right]$$
$$= a_1 - a_2, \tag{F23}$$

where

$a_1 = \left[\frac{2\pi\beta r_I (c+\beta\overline{T}^0)^2}{r_T} + \frac{2\beta\pi c\mu K}{r_T \overline{T}^0} \left(\frac{K\rho(c+\beta\overline{T}^0)}{r_P(\overline{T}^0 - \overline{P}^0)} \right) \right],$

$a_2 = \left[\frac{2K\rho r_I \mu (c+\beta\overline{T}^0)^3}{r_T r_P \overline{T}^0 (\overline{T}^0 - \overline{P}^0)} + 2\beta\pi c \left(c + \beta\overline{T}^0 + \frac{K\rho(c+\beta\overline{T}^0)}{r_P(\overline{T}^0 - \overline{P}^0)} + \frac{\pi\beta K}{r_T} \right) \right].$

Hence, $a > 0$ if and only if

$$a_1 > a_2, \tag{F24}$$

and $a < 0$ if and only if

$$a_1 < a_2. \tag{F25}$$

Computation of b: Similarly, to compute b, we need to find the following partial derivatives,

$$\frac{\partial^2 f_2}{\partial x_1 \partial \delta} = 0, \ \frac{\partial^2 f_2}{\partial x_2 \partial \delta} = -1, \ \frac{\partial^2 f_2}{\partial x_3 \partial \delta} = 0, \ \frac{\partial^2 f_2}{\partial x_4 \partial \delta} = 0,$$
$$\frac{\partial^2 f_4}{\partial x_1 \partial \delta} = 0, \ \frac{\partial^2 f_4}{\partial x_2 \partial \delta} = 0, \ \frac{\partial^2 f_4}{\partial x_3 \partial \delta} = 0, \ \frac{\partial^2 f_4}{\partial x_4 \partial \delta} = 0,$$

Substituting the vectors $\mathbf{v}$ defined in equation(F21) and $\mathbf{w}$ defined in equation(F22) and the respective partial derivatives (evaluated at the IFE $\mathcal{E}_0$) into the expression,

$$b = \sum_{i,k=1}^{4} v_k w_i \frac{\partial^2 f_k(0,0)}{\partial x_i \partial \alpha}$$

After some algebraic manipulation, we obtain

$$b = -w_2 v_2 = -(c+\beta\overline{T}^0)^2 < 0. \tag{F26}$$

Therefore, b is always negative. Meanwhile a is positive if condition F24 holds and negative if condition F25 holds. Thus, by Theorem 4.1 [34] we have a backward bifurcation under condition F24 and a forward bifurcation under condition F25. This completes the proof. □

Appendix G

Proof of Theorem 7: The Hurwitz determinants obtained from the characteristic polynomial Eq. (10), H_i, are

$$\begin{aligned} H_1 &= A_1, \\ H_2 &= A_1 A_2 - A_3, \\ H_3 &= A_1 A_2 A_3 - A_1^2 A_4 - A_3^2, \\ H_4 &= A_4 H_3. \end{aligned} \tag{G27}$$

The generalized Routh-Hurwitz criterion indicates that $\mathcal{E}^\dagger$ is locally asymptotically stable if and only if $H_i > 0 \ \forall i$ and that a necessary condition for the existence of a Hopf bifurcation is [50]

$$H_1 > 0, \ H_2 > 0, \ H_3\|_{\delta_h} = 0, \text{ and } \frac{d}{d\delta}(H_3\|_{\delta_h}) \neq 0, \tag{G28}$$

where δ_h is the Hopf bifurcation parameter. This simplifies to

$$A_1 A_2 A_3 - A_1^2 A_4 - A_3^2 = 0. \tag{G29}$$

This completes the proof. □

References

[1] A. Schweitzer, J. Horn, R. T. Mikolajczyk, G. Krause, J. J. Ott, Estimations of worldwide prevalence of chronic hepatitis B virus infection: a systematic review of data published between 1965 and 2013, The Lancet 386 (10003) (2015) 1546–1555.

[2] L. G. Guidotti, F. V. Chisari, Immunobiology and pathogenesis of viral hepatitis, Annu. Rev. Pathol. Mech. Dis. 1 (2006) 23–61.

[3] W. M. Lee, Hepatitis B virus infection, New England journal of medicine 337 (24) (1997) 1733–1745.

[4] S. Locarnini, A. Hatzakis, D.-S. Chen, A. Lok, Strategies to control hepatitis B: Public policy, epidemiology, vaccine and drugs, Journal of hepatology 62 (1) (2015) S76–S86.

[5] M.-F. Yuen, D.-S. Chen, G. M. Dusheiko, H. L. Janssen, D. T. Lau, S. A. Locarnini, M. G. Peters, C.-L. Lai, Hepatitis B virus infection, Nature reviews Disease primers 4 (1) (2018) 1–20.

[6] K.-N. Tsai, C.-F. Kuo, J.-H. J. Ou, Mechanisms of hepatitis B virus persistence, Trends in microbiology 26 (1) (2018) 33–42.

[7] S. F. Wieland, F. V. Chisari, Stealth and cunning: hepatitis B and hepatitis C viruses, Journal of virology 79 (15) (2005) 9369–9380.

[8] E. T. Tjwa, G. W. van Oord, J. P. Hegmans, H. L. Janssen, A. M. Woltman, Viral load reduction improves activation and function of natural killer cells in patients with chronic hepatitis B, Journal of hepatology 54 (2) (2011) 209–218.

[9] R. G. van der Molen, D. Sprengers, R. S. Binda, E. C. de Jong, H. G. Niesters, J. G. Kusters, J. Kwekkeboom, H. L. Janssen, Functional impairment of myeloid and plasmacytoid dendritic cells of patients with chronic hepatitis B, Hepatology 40 (3) (2004) 738–746.

[10] Y. Kondo, M. Ninomiya, E. Kakazu, O. Kimura, T. Shimosegawa, Hepatitis B surface antigen could contribute to the immunopathogenesis of hepatitis B virus infection, International Scholarly Research Notices 2013 (2013).

[11] S. Asabe, S. F. Wieland, P. K. Chattopadhyay, M. Roederer, R. E. Engle, R. H. Purcell, F. V. Chisari, The size of the viral inoculum contributes to the outcome of hepatitis B virus infection, Journal of virology 83 (19) (2009) 9652–9662.

[12] Z. Zeng, L. Li, Y. Chen, H. Wei, R. Sun, Z. Tian, Interferon-γ facilitates hepatic antiviral T cell retention for the maintenance of liver-induced systemic tolerance, Journal of Experimental Medicine 213 (6) (2016) 1079–1093.

[13] J. R. Moore, H. Ahmed, B. Manicassamy, A. Garcia-Sastre, A. Handel, R. Antia, Varying inoculum dose to assess the roles of the immune response and target cell depletion by the pathogen in control of acute viral infections, Bulletin of mathematical biology 82 (2020) 1–14.

[14] S. M. Ciupe, N. K. Vaidya, J. E. Forde, Early events in hepatitis B infection: The role of inoculum dose, Proceedings of the Royal Society B

288 (1944) (2021) 20202715.

[15] S. M. Ciupe, Modeling the dynamics of hepatitis B infection, immunity, and drug therapy, Immunological Reviews 285 (1) (2018) 38–54.

[16] H. Dahari, E. Shudo, R. M. Ribeiro, A. S. Perelson, Modeling complex decay profiles of hepatitis B virus during antiviral therapy, Hepatology 49 (1) (2009) 32–38.

[17] N. K. Vaidya, R. M. Ribeiro, C. J. Miller, A. S. Perelson, Viral dynamics during primary simian immunodeficiency virus infection: effect of time-dependent virus infectivity, Journal of virology 84 (9) (2010) 4302–4310.

[18] S. M. Ciupe, C. J. Miller, J. E. Forde, A bistable switch in virus dynamics can explain the differences in disease outcome following SIV infections in rhesus macaques, Frontiers in microbiology 9 (2018) 348818.

[19] Y. Li, A. Handel, Modeling inoculum dose dependent patterns of acute virus infections, Journal of theoretical biology 347 (2014) 63–73.

[20] S. Baral, R. Antia, N. M. Dixit, A dynamical motif comprising the interactions between antigens and CD8 T cells may underlie the outcomes of viral infections, Proceedings of the National Academy of Sciences 116 (35) (2019) 17393–17398.

[21] S. M. Ciupe, J. M. Conway, Incorporating intracellular processes in virus dynamics models, Microorganisms 12 (5) (2024) 900.

[22] A. Goyal, L. E. Liao, A. S. Perelson, Within-host mathematical models of hepatitis B virus infection: Past, present, and future, Current Opinion in Systems Biology 18 (2019) 27–35.

[23] S. M. Ciupe, J. M. Heffernan, In-host modeling, Infectious Disease Modelling 2 (2) (2017) 188–202.

[24] S. M. Ciupe, J. E. Forde, Virus dynamics, Case Studies in Systems Biology (2021) 245–261.

[25] S. M. Ciupe, R. M. Ribeiro, P. W. Nelson, A. S. Perelson, Modeling the mechanisms of acute hepatitis B virus infection, Journal of theoretical biology 247 (1) (2007) 23–35.

[26] S. M. Ciupe, R. M. Ribeiro, P. W. Nelson, G. Dusheiko, A. S. Perelson, The role of cells refractory to productive infection in acute hepatitis B viral dynamics, Proceedings of the National Academy of Sciences 104 (12) (2007) 5050–5055.

[27] A. Carracedo Rodriguez, M. Chung, S. M. Ciupe, Understanding the complex patterns observed during hepatitis B virus therapy, Viruses 9 (5) (2017) 117.

[28] S. M. Ciupe, R. M. Ribeiro, A. S. Perelson, Antibody responses during hepatitis B viral infection, PLoS computational biology 10 (7) (2014) e1003730.

[29] H. Gulbudak, J. S. Weitz, Heterogeneous viral strategies promote coexistence in virus-microbe systems, Journal of theoretical biology 462 (2019) 65–84.

[30] H. Gulbudak, P. L. Salceanu, G. S. Wolkowicz, A delay model for persistent viral infections in replicating cells, Journal of Mathematical Biology

82 (7) (2021) 59.

[31] J. C. Macdonald, H. Gulbudak, Forward hysteresis and hopf bifurcation in an npzd model with application to harmful algal blooms, Journal of Mathematical Biology 87 (3) (2023) 45.

[32] J. S. Weitz, G. Li, H. Gulbudak, M. H. Cortez, R. J. Whitaker, Viral invasion fitness across a continuum from lysis to latency, Virus evolution 5 (1) (2019) vez006.

[33] H. Gulbudak, M. Martcheva, Forward hysteresis and backward bifurcation caused by culling in an avian influenza model, Mathematical biosciences 246 (1) (2013) 202–212.

[34] C. Castillo-Chavez, B. Song, Dynamical models of tuberculosis and their applications, Mathematical Biosciences & Engineering 1 (2) (2004) 361–404.

[35] M.-P. Bralet, S. Branchereau, C. Brechot, N. Ferry, Cell lineage study in the liver using retroviral mediated gene transfer. evidence against the streaming of hepatocytes in normal liver, The American journal of pathology 144 (5) (1994) 896.

[36] F. Brauer, C. Castillo-Chavez, C. Castillo-Chavez, Mathematical models in population biology and epidemiology, Vol. 2, Springer, 2012.

[37] S. M. Ciupe, A. J. Catllá, J. Forde, D. G. Schaeffer, Dynamics of hepatitis B virus infection: what causes viral clearance?, Mathematical Population Studies 18 (2) (2011) 87–105.

[38] J. E. Forde, S. M. Ciupe, A. Cintron-Arias, S. Lenhart, Optimal control of drug therapy in a hepatitis B model, Applied Sciences 6 (8) (2016) 219.

[39] J. Summers, A. R. Jilbert, W. Yang, C. E. Aldrich, J. Saputelli, S. Litwin, E. Toll, W. S. Mason, Hepatocyte turnover during resolution of a transient hepadnaviral infection, Proceedings of the National Academy of Sciences 100 (20) (2003) 11652–11659.

[40] C. Ferrari, A. Penna, A. Bertoletti, A. Valli, A. D. Antoni, T. Giuberti, A. Cavalli, M. A. Petit, F. Fiaccadori, Cellular immune response to hepatitis B virus-encoded antigens in acute and chronic hepatitis B virus infection., Journal of immunology (Baltimore, Md.: 1950) 145 (10) (1990) 3442–3449.

[41] R. C. Hoogeveen, S. Dijkstra, L. M. Bartsch, H. K. Drescher, J. Aneja, M. P. Robidoux, J. A. Cheney, J. Timm, A. Gehring, P. S. F. de Sousa, et al., Hepatitis B virus-specific CD4 T cell responses differentiate functional cure from chronic surface antigen+ infection, Journal of hepatology 77 (5) (2022) 1276–1286.

[42] A. Bertoletti, C. Ferrari, Adaptive immunity in hbv infection, Journal of hepatology 64 (1) (2016) S71–S83.

[43] S. M. Ciupe, S. Hews, Mathematical models of e-antigen mediated immune tolerance and activation following prenatal HBV infection, PLoS One 7 (7) (2012) e39591.

[44] S. Kadelka, S. M Ciupe, Mathematical investigation of HBeAg seroclearance, Mathematical Biosciences and Engineering 16 (6) (2019).

[45] K. Kitagawa, K. S. Kim, M. Iwamoto, S. Hayashi, H. Park, T. Nishiyama, N. Nakamura, Y. Fujita, S. Nakaoka, K. Aihara, et al., Multiscale modeling of HBV infection integrating intra-and intercellular viral propagation to analyze extracellular viral markers, PLOS Computational Biology 20 (3) (2024) e1011238.

[46] S. El Messaoudi, A. Lemenuel-Diot, A. Gonçalves, J. Guedj, A semi-mechanistic model to characterize the long-term dynamics of hepatitis B virus markers during treatment with lamivudine and pegylated interferon, Clinical Pharmacology & Therapeutics 113 (2) (2023) 390–400.

[47] S. Kadelka, H. Dahari, S. M. Ciupe, Understanding the antiviral effects of RNAi-based therapy in HBeAg-positive chronic hepatitis B infection, Scientific Reports 11 (1) (2021) 200.

[48] O. Diekmann, J. A. P. Heesterbeek, Mathematical epidemiology of infectious diseases: model building, analysis and interpretation, Vol. 5, John Wiley & Sons, 2000.

[49] J. Carr, Applications of centre manifold theory, Vol. 35, Springer Science & Business Media, 2012.

[50] W.-M. Liu, Criterion of Hopf bifurcations without using eigenvalues, Journal of Mathematical Analysis and Applications 182 (1) (1994) 250–256.